NEUROSCIENCE

Corticotropin-releasing hormone neurons control trigeminal neuralgia-induced anxiodepression via a hippocampus-to-prefrontal circuit

Su-Su Lv, Xue-Jing Lv, Ya-Qi Cai, Xin-Yu Hou, Zhi-Zhe Zhang, Guo-Hong Wang, Li-Qiang Chen, Ning Lv, Yu-Qiu Zhang*

Anxiety and depression are frequently observed in patients suffering from trigeminal neuralgia (TN), but neural circuits and mechanisms underlying this association are poorly understood. Here, we identified a dedicated neural circuit from the ventral hippocampus (vHPC) to the medial prefrontal cortex (mPFC) that mediates TN-related anxiodepression. We found that TN caused an increase in excitatory synaptic transmission from vHPC^{CaMK2A} neurons to mPFC inhibitory neurons marked by the expression of corticotropin-releasing hormone (CRH). Activation of CRH^{+} neurons subsequently led to feed-forward inhibition of layer V pyramidal neurons in the mPFC via activation of the CRH receptor 1 (CRHR1). Inhibition of the vHPC^{CaMK2A}-mPFC^{CRH} circuit ameliorated TN-induced anxiodepression, whereas activating this pathway sufficiently produced anxiodepressive-like behaviors. Thus, our studies identified a neural pathway driving pain-related anxiodepression and a molecular target for treating pain-related psychiatric disorders.

INTRODUCTION

Mood disorders such as depression and anxiety are frequently observed in patients suffering from chronic pain, affecting quality of life and increasing the burden on health care services for patients (*1*). Among patients with chronic pain, the prevalence rates of major depression are reported to range from 18 to 85% (*2*, *3*). In particular, this comorbidity may lead to a vicious cycle of pain and anxiodepression symptoms (*4*). Neuroimaging studies in humans and model animals of chronic pain have revealed changes in structural and functional connectivity of corticolimbic brain areas, including the medial prefrontal cortex (mPFC), orbitofrontal cortex, amygdala, and hippocampus (*5*–*7*). These nuclei are also relevant to neuropsychiatric disorders, such as anxiety and depression (*8*, *9*). Emerging evidence has demonstrated that both ventral hippocampus (vHPC) and mPFC, as well as their connectivity, are necessary for a variety of behavioral challenges including fear (*10*), anxiety (*11*, *12*), and pain (*13*, *14*). However, it is unclear whether and how the network activity between the vHPC and the mPFC mediates and modulates the pain-related anxiodepressive-like emotions.

The vHPC projections to the mPFC have been identified (*15*) and have been reported to be implicated in the expression and extinction of emotional memories such as fear memory (*16*, *17*). In terms of learning and memory, chronic pain can be viewed as a state of continuous learning and a persistence of the memory of pain, in which negative emotional associations are continuously established with daily pain episodes (*18*). It has been previously demonstrated that the anxiodepressive-like consequences of neuropathic pain evolve in a time-dependent manner (*19*, *20*). Our recent study has also demonstrated that mechanical hypersensitivity occurs immediately following trigeminal neuralgia (TN), whereas anxiodepressive-like behaviors are observed 14 days (14d) later (*21*). The delayed development of anxiodepressive-like emotions may be attributed to the retrieval and consolidation of negative emotional memories related to pain episodes evoked by daily activities such as eating, drinking, and licking. Thus, we therefore postulate that the vHPC-mPFC projections may also be required for the development of anxiodepressive-like behaviors in TN mice.

Decreased activity of pyramidal output neurons in the mPFC has been implicated in the development of psychiatric disorders (*22*, *23*). In this study, combining genetic and pharmacological approaches, we have now demonstrated that corticotropin-releasing hormone [CRH; also called corticotropin-releasing factor (CRF)] neurons, as a unique subtype of GABAergic inhibitory interneurons in the mPFC, directly receive excitatory projections from the vHPC and are required to drive chronic pain–induced anxiety and depression via feed-forward inhibition of the major output neurons in the mPFC. Our studies further suggested that the associated CRH–CRH receptor 1 (CRHR1) signaling could be a target for treating anxiodepressive consequences of chronic pain.

RESULTS

TN decreases activity of layer V mPFC pyramidal neurons in a time-dependent manner

We previously showed that TN mice exhibit obvious anxiodepressive-like behaviors by 14 days but not 4 day after chronic constriction injury of the infraorbital nerve (CION), indicating that anxiodepressive-like behaviors caused by neuropathic pain were time dependent (*21*). In this study, we investigated whether TN altered the excitability and synaptic transmission of mPFC neurons accompanying the anxiodepressive-like behaviors. As layer V provides the main integrated output of the mPFC (*24*), we recorded neural activity of layer V pyramidal neurons in mPFC slices from sham, CION-4d, and CION-14d mice (Fig. 1A). Action potentials (APs) were evoked by 10-pA step depolarizing current pulses ranging from 0 to 200 pA. The input-output curves appeared right-shifted with a more depolarized AP firing

Department of Translational Neuroscience, Jing'an District Centre Hospital of Shanghai, State Key Laboratory of Medical Neurobiology and MOE Frontiers Center for Brain Science, Institutes of Brain Science, Fudan University, Shanghai 200032, China.
*Corresponding author. Email: yuqiuzhang@fudan.edu.cn

threshold and more hyperpolarized rest membrane potential (RMP) at day 14 but not day 4 after CION (Fig. 1, B to F), indicating that the intrinsic excitability of layer V pyramidal neurons was decreased following TN development in a time-dependent manner. We further recorded spontaneous excitatory postsynaptic currents (sEPSCs) and spontaneous inhibitory postsynaptic currents (sIPSCs) in mPFC layer V pyramidal neurons. CION induced a notable increase in amplitude and an increasing trend in frequency of sIPSCs, whereas sEPSCs remained unchanged, indicating an enhanced inhibitory synaptic transmission of layer V pyramidal neurons (Fig. 1, G to L). To determine whether the decrease in excitability of layer V pyramidal neurons in CION mice depends on enhanced inhibitory inputs, we examined the effect of blocking γ-aminobutyric acid type A ($GABA_A$) receptors on the excitability of layer V mPFC pyramidal neurons. A leftward shift in input-output curves of APs was observed after bath perfusion of $GABA_A$ receptor inhibitor bicuculline (BIC; 10 μM; fig. S1), suggesting that the increase in inhibitory inputs contributes to the decrease in excitability of layer V pyramidal neurons in TN mice. Thus, the decrease in neuronal activity of layer V pyramidal neuron following TN may be due to both a decrease intrinsic excitability and an increase in inhibitory inputs.

Enhanced neuronal activity in the vHPC drives feed-forward inhibition of layer V pyramidal neurons

We next explored the presynaptic source that drove enhanced inhibitory inputs onto layer V pyramidal neurons in the mPFC. mPFC received inputs from various brain regions, including the vHPC whose plasticity

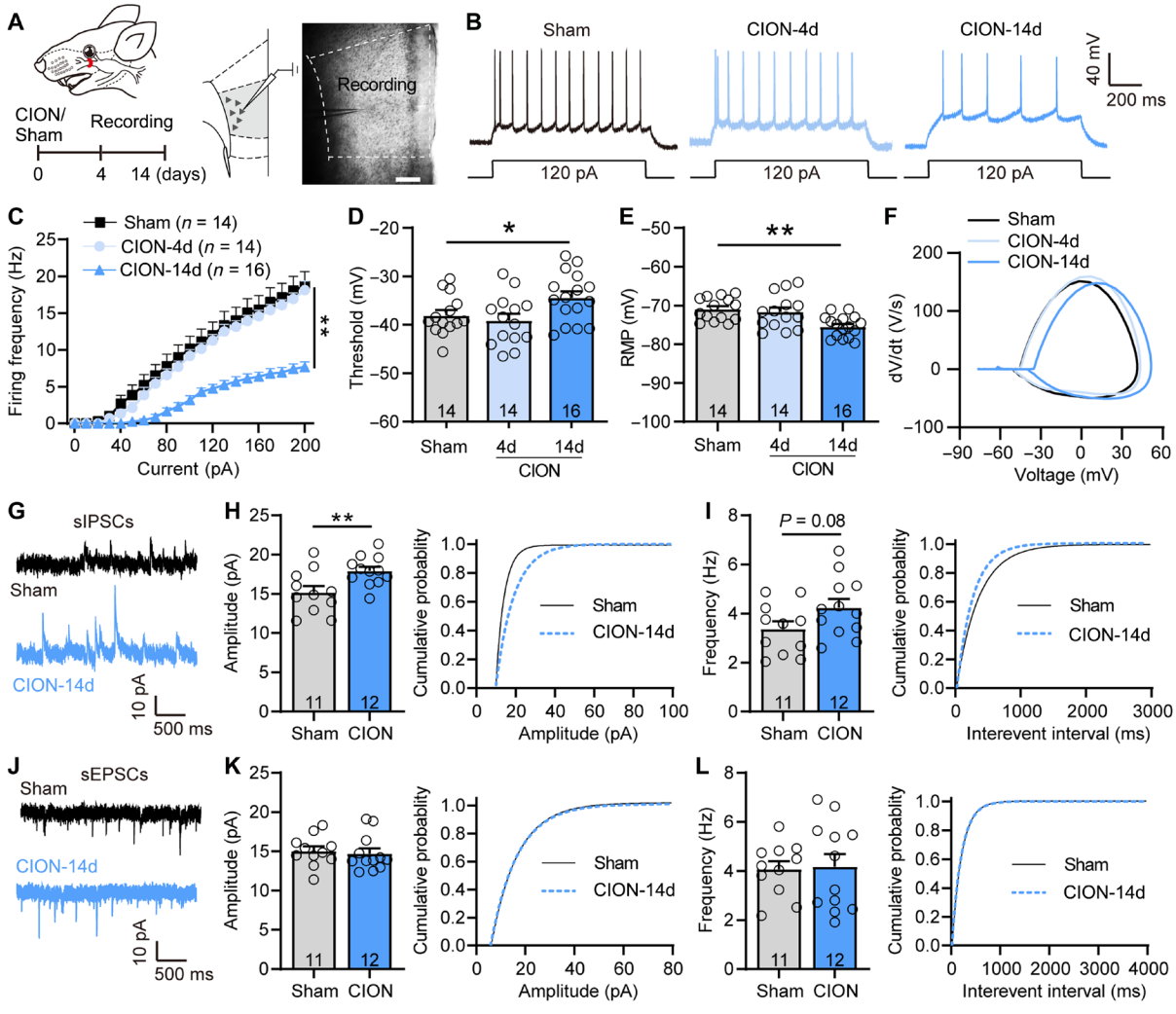

Fig. 1. TN decreases the excitability and increases inhibitory synaptic transmission of layer V mPFC pyramidal neurons. (**A**) Schematic showing chronic CION and mPFC slice image showing the location of the recorded neurons in layer V mPFC pyramidal neurons. Scale bar, 200 μm. (**B**) Examples of AP traces evoked by depolarizing current in layer V mPFC pyramidal neurons from sham, CION-4d, and CION-14d mice. (**C**) CION time dependently decreases firing frequency of APs evoked by depolarizing current steps in mPFC layer V pyramidal neurons. $^{**}P < 0.01$, two-way repeated measure (RM) ANOVA. (**D** and **E**) CION-14d mice have more depolarized AP firing threshold (D) and more hyperpolarized RMP (E) in layer V mPFC pyramidal neurons, compared with sham and CION-4d ones. $^{*}P < 0.05$, $^{**}P < 0.01$, one-way ANOVA. (**F**) Phase plots of the APs evoked by brief current injections in mPFC layer V pyramidal neurons from sham, CION-4d, and CION-14d mice. (**G** to **I**) Patch clamp recording of sIPSCs showing an increased amplitude of sIPSCs and a right-shifted cumulative fraction in layer V mPFC pyramidal neurons from CION-14d mice. $^{**}P < 0.01$, two-tailed Student's *t* test. (**J** to **L**) Patch clamp recording of sEPSCs showing no difference in amplitude and frequency of sEPSCs in layer V mPFC pyramidal neurons. Two-tailed Student's *t* test. Data are expressed as means ± SEM. Sample sizes are indicated in bars and parentheses. See also fig. S1.

has been implicated in psychiatric disorders (*12*, *25*). We first verified projections from the vHPC to the mPFC by injecting adeno-associated virus (AAV)–calcium/calmodulin-dependent protein kinase II alpha (CaMK2A)–channelrodopsin-2 (ChR2) into the CA1 region of the vHPC (Fig. 2, A and B). Then, we labeled mPFC-projecting vHPC CaMK2A$^+$ neurons by injecting AAV-retro-mCherry into the mPFC and recorded the neuronal activity of these presynaptic neurons in vHPC slices (Fig. 2C). Corresponding to the time window of decreased excitatory activity of layer V mPFC pyramidal neurons and the development of anxiodepressive-like behaviors, the changes of intrinsic excitability and membrane properties of mPFC-projecting vHPC neurons were also observed on day 14 but not day 4 after CION. The input-output curves of APs in vHPC CaMK2A$^+$ neurons appeared left-shifted with a more hyperpolarized AP firing threshold and a more depolarized RMP at day 14 after CION (Fig. 2, D to H), indicating that the excitability of mPFC-projecting vHPC neurons was increased following TN development. We further used fiber photometry to measure anxiety state–induced changes in Ca^{2+} signals in vHPC CaMK2A$^+$ neurons expressing the Ca^{2+} indicator green fluorescent protein fused to a calmodulin protein (GCaMP6s). Increased neuronal activity of vHPC

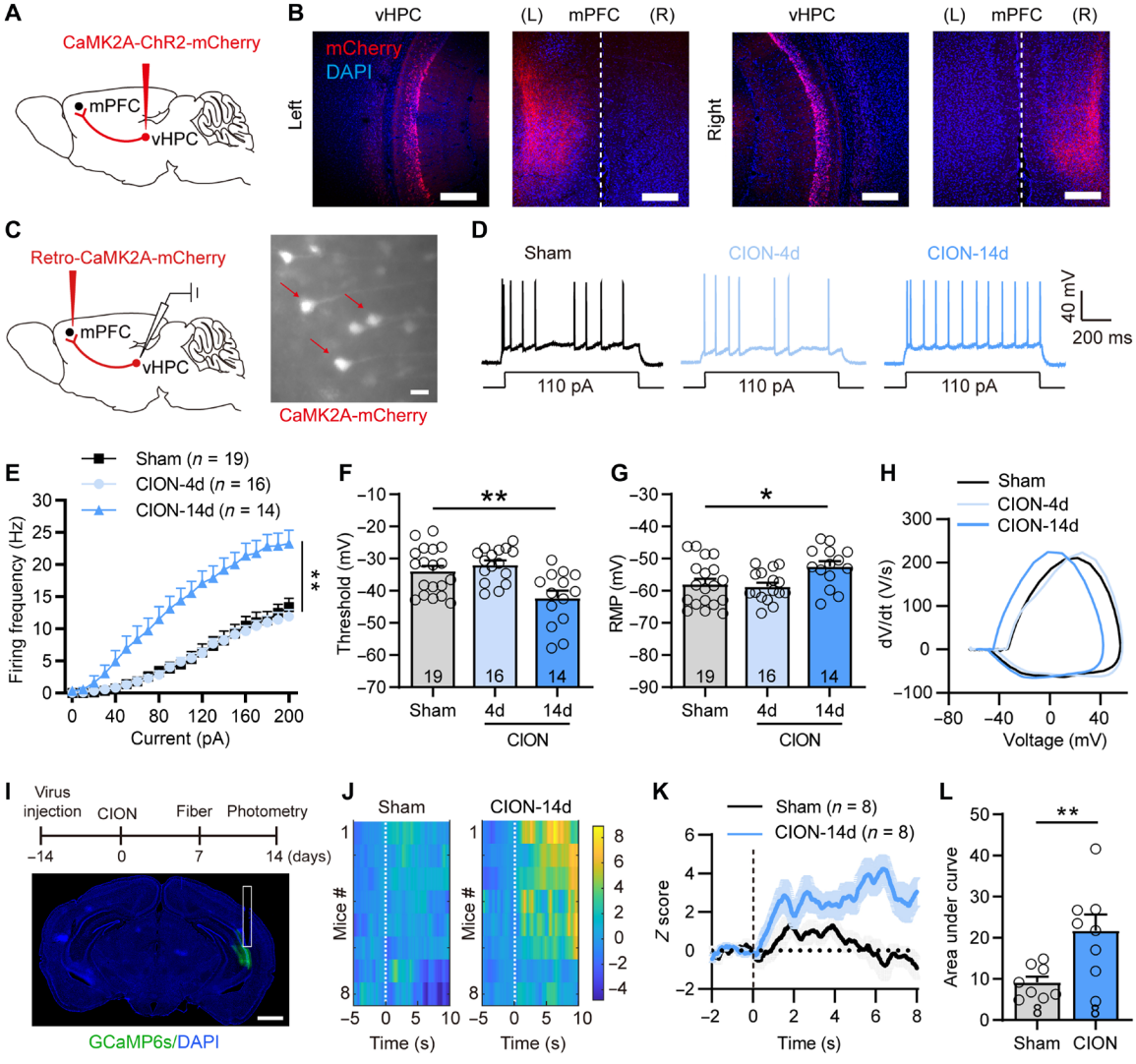

Fig. 2. TN increases excitatory activity of mPFC-projecting CaMK2A$^+$ vHPC pyramidal neurons. (**A** and **B**) Sagittal schematic showing AV-CaMK2A-ChR2-mCherry injection into the vHPC, and fluorescent signals were detected in the mPFC after intra-vHPC virus injection. Scale bars, 200 μm. (**C**) Sagittal schematic showing specific infection of mCherry on mPFC-projecting CaMK2A$^+$ neurons in the vHPC and vHPC slice image showing the recorded CaMK2A$^+$ neurons. Scale bar, 30 μm. (**D**) Examples of AP traces evoked by depolarizing current in vHPC CaMK2A$^+$ neurons from sham, CION-4d, and CION-14d mice. (**E**) CION increases firing frequency of APs evoked by depolarizing current steps in vHPC CaMK2A$^+$ neurons on day 14 but not on day 4. $^{**}P < 0.01$, two-way RM ANOVA. (**F** and **G**) CION-14d mice have more hyperpolarized AP firing threshold (F) and more depolarized RMP (G) in vHPC CaMK2A$^+$ neurons. $^{*}P < 0.05$, $^{**}P < 0.01$, one-way ANOVA. (**H**) Phase plots of the APs evoked by brief current injections in vHPC CaMK2A$^+$ neurons from sham, CION-4d, and CION-14d mice. (**I**) Schematic and photomicrograph of coronal section showing the protocol for in vivo optical fiber photometry recording (top) and the sites of optical fiber implantation and CaMK2A-GCaMP6s expression in the vHPC (bottom). Scale bar, 1 mm. (**J** to **L**) Heatmap of fluorescence (J), mean fluorescence of Ca^{2+} transients (K), and area under curve of changes in Ca^{2+} transients (L) showing robustly increased neuronal activity of vHPC CaMK2A$^+$ neurons when mice moved from closed arm to open arm in EPM on day 14 after CION. $^{**}P < 0.01$, two-tailed Student's *t* test. Data are expressed as means ± SEM. Sample sizes are indicated in bars and parentheses. See also fig. S2. DAPI, 4′,6-diamidino-2-phenylindole.

$CaMK2A^+$ neurons was observed when mice moved from the closed arm to the open arm in an elevated plus maze (EPM). The elevated Ca^{2+} activity in CION mice was greater than that of sham mice (Fig. 2, I to L). The sIPSCs and sEPSCs of vHPC $CaMK2A^+$ neurons from sham and CION-14d mice were also recorded. CION-14d mice exhibited an increased amplitude of sEPSCs, further supporting that TN enhanced the excitability of vHPC $CaMK2A^+$ neurons on day 14 (fig. S2).

To determine whether the decreased activity of layer V mPFC pyramidal neurons is attributed to the increased vHPC excitatory inputs (via more dominant feed-forward activation of inhibitory neurons, see below), we activated vHPC-mPFC projections and then measured the effect on the activity of layer V mPFC pyramidal neurons. Following optogenetic activation of vHPC $CaMK2A^+$ presynaptic terminals in the mPFC, both optoactivated EPSC (oEPSC) and optoactivated IPSC (oIPSC) were recorded in mPFC layer V pyramidal neurons (Fig. 3, A and B). The oIPSC amplitude and ratio of oIPSC/oEPSC in CION-14d mice were significantly higher than that in the sham controls (Fig. 3, C and D), indicating that CION shifted excitatory-inhibitory (E-I) balance of $vHPC^{CaMK2A}$-mPFC pathway toward inhibition in mPFC layer V pyramidal neurons. Consistent with increased inhibitory inputs, optogenetic activation of vHPC $CaMK2A^+$ presynaptic terminals in the mPFC led to a rightward shift in the input-output curves of APs and significantly suppressed AP firing frequency of layer V pyramidal neurons evoked by ramp depolarizing current (Fig. 3, E to H). Bath perfusion of BIC (10 μM) blocked the effect of optogenetic activation of vHPC $CaMK2A^+$ presynaptic terminals on AP firing (Fig. 3, I and J). To determine direct or indirect inputs from vHPC to mPFC, we additionally performed voltage-clamp recording from mPFC layer V pyramidal neurons, showing that both oEPSC and oIPSC were completely abolished by voltage-gated Na^+ channel blocker tetrodotoxin (TTX; 1 μM), whereas only oEPSC, rather than oIPSC, could be rescued by voltage-gated K^+ channel blocker 4-aminopyridine (4-AP; 100 μM) in the presence of TTX, under which voltage-sensitive Ca^{2+} channel can gain the ability to drive depolarization and glutamate release (Fig. 3K) (*26*), indicating that the oEPSCs but not oIPSCs were elicited by direct synaptic connections between vHPC $CaMK2A^+$ neurons and mPFC layer V pyramidal neurons. Moreover, both oEPSC and oIPSC were completely eliminated by AMPA receptor antagonist 6-cyano-7-nitroquinoxaline-2,3-dione (CNQX; 10 μM; Fig. 3L). These results indicate that layer V mPFC pyramidal neurons receive direct excitatory inputs from $vHPC^{CaMK2A}$ neurons, but these inputs were dominantly inhibited via feed-forward activation of mPFC inhibitory interneurons, particularly under the TN condition (Fig. 3M).

Together with our previous study showing that TN mice developed anxiodepressive-like behaviors in 14 days but not 4 day after CION, we postulated that increased excitatory activity of vHPC $CaMK2A^+$ neurons and the decreased excitatory activity of layer V mPFC pyramidal neurons on 14th day of CION may be associated with the development of anxiodepressive-like behaviors, and we subsequently conducted a series of studies to test this hypothesis (see below).

Anxiodepressive consequences of TN require $vHPC^{CaMK2A}$-$mPFC^{vGat}$ projections

We next investigated the role of the $vHPC^{CaMK2A}$-mPFC inputs in driving TN-associated anxiodepression. We injected the antegrade-tracing AAV2/1-hSyn-Cre virus into the vHPC and Cre-dependent AAV–double-floxed inverse orientation (DIO)–enhanced green fluorescent protein (EGFP) virus into the mPFC (Fig. 4A and fig. S3A), such that AAV2/1-Cre from transduced presynaptic neurons can effectively and specifically drive Cre-dependent transgene expression in selected postsynaptic neuronal targets (*27*). RNAscope fluorescence in situ hybridization (FISH) identified *vGat*-positive postsynaptic neurons in the mPFC, confirming the direct projections from the vHPC to mPFC GABAergic neurons (Fig. 4B). Moreover, c-Fos immunohistochemical staining showed that following optogenetic activation of $vHPC^{CaMK2A}$-mPFC projection terminals, more than 40% of *vGat*-positive mPFC neurons were activated (fig. S3, B and C), suggesting a functional connection between vHPC excitatory outputs and mPFC inhibitory interneurons. To determine the effects of $vHPC\text{-}mPFC^{GABA}$ pathway on CION-induced anxiodepressive-like behaviors, we injected AAV2/1-hsyn-Cre into the vHPC and AAV2/9-Gad67-DIO-hM4Di into the mPFC to inhibit postsynaptic mPFC GABAergic inhibitory neurons receiving vHPC projections (Fig. 4, C and D, and fig. S3A). Intraperitoneal injection of CNO (5 mg/kg, 0.1 ml) was used specifically to inhibit hM4Di-expressing $Gad67^+$ postsynaptic GABAergic neurons in the mPFC receiving vHPC projections. This silence of inhibitory neuron activity produced anti-anxiodepressive–like effects, as indicated by an increase in open arm entries and open arm staying time in the EPM test, as well as by an increase in center-traveling distance in the open field (OF) test, less immobile time in the tail suspension (TS) test, and more sucrose consumption in the sucrose preference (SP) test (Fig. 4, E to K). Notably, inhibition of vHPC-mPFC postsynaptic $Gad67^+$ neurons has no effect on CION-induced mechanical hypersensitivity in the vibrissa pad (Fig. 4L). These results imply that the feed-forward inhibition mediated by mPFC GABAergic inhibitory neurons receiving projections from the vHPC may be specifically involved in CION-induced anxiodepressive-like behaviors.

To further confirm this conclusion, we also took an alternative optogenetic approach to inhibit $vHPC^{CaMK2A}$-mPFC pathway. To do so, we performed intra-vHPC injection of AAV–encoding halorhodopsin (eNpHR)–enhanced yellow fluorescent protein (EYFP) virus driven by the CaMK2A promoter in CION mice (fig. S3D). Yellow light stimulation (583 nm, 10 mW, continuous) of the presynaptic terminals of $vHPC^{CaMK2A}$ neurons in the mPFC significantly alleviated TN-induced anxiodepressive-like behaviors (fig. S3, E to K). The anti-anxiodepressive effect of inhibiting vHPC-mPFC postsynaptic $vGat^+$ neurons or $vHPC^{CaMK2A}$-mPFC terminals could also be mimicked by optogenetic soma inhibition of vHPC $CaMK2A^+$ neurons (fig. S4, A to G). Our previous study showed that inhibition of microglia in the ipsilateral but not the contralateral dorsal hippocampus (dHPC) blocked CION-induced anxiodepressive-like behaviors, suggesting an asymmetric role of dHPC (*21*). However, unlike manipulating dHPC microglia, there was no significant difference in the anti-anxiodepressive effects of silencing ipsilateral and contralateral vHPC $CaMK2A^+$ neurons (fig. S4, A to G).

Considering that either inhibitory interneurons or excitatory pyramidal neurons receive direct excitatory inputs from $vHPC^{CaMK2A}$ neurons (as shown in Fig. 3M), we also examined the effects of vHPC-mPFC excitatory postsynaptic neurons on CION-induced anxiodepressive-like behaviors. RNAscope FISH and c-Fos immunohistochemical results showed a functional connection between vHPC excitatory outputs and mPFC excitatory neurons (fig. S5, A to D). Optogenetic inhibition of vHPC-mPFC $CaMK2A^+$ excitatory postsynaptic neurons did not affect CION-induced anxiodepressive-like behaviors (fig. S5, E to K). Collectively, the above data indicate that vHPC excitatory outputs to mPFC inhibitory neurons are necessary for the manifestation of TN-induced anxiodepressive-like behaviors.

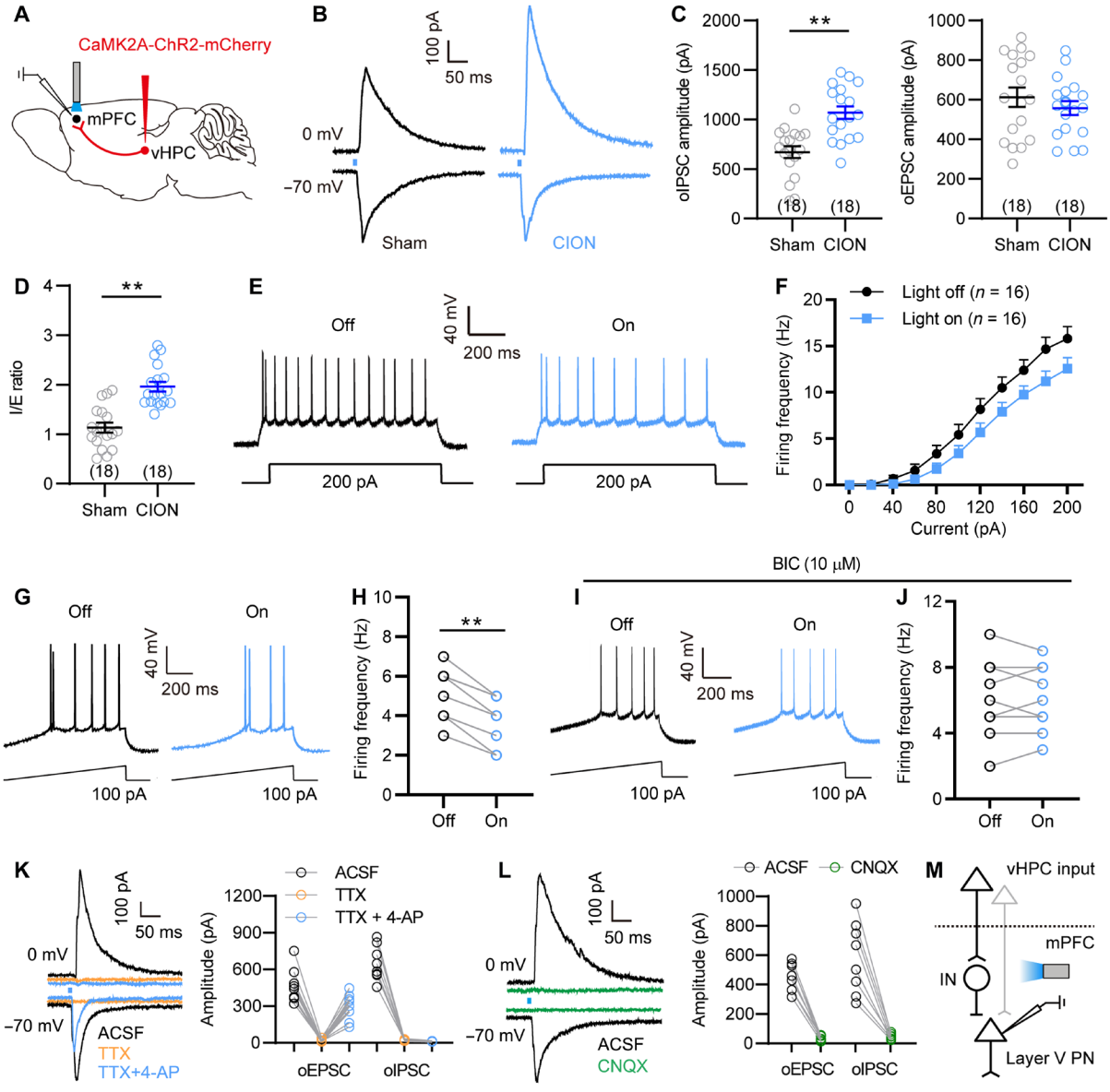

Fig. 3. vHPC excitatory inputs decrease neuronal activity of mPFC layer V pyramidal neurons through feed-forward inhibition. (**A**) Schematic showing AAV-CaMK2A-ChR2-mCherry injection into the vHPC, optogenetic activation of vHPC^{CaMK2A}-positive terminals and whole-cell recording of layer V pyramidal neurons in the mPFC. (**B**) Representative traces showing the oEPSC and oIPSC in layer V mPFC pyramidal neurons from sham and CION-14d mice following light activation of vHPC-^{CaMK2A} inputs. (**C** and **D**) CION increases oIPSC amplitude and IPSC/EPSC (I/E) ratio. $^{**}P < 0.01$, two-tailed Student's *t* test. (**E** and **F**) Optogenetic activation of vHPC^{CaMK2A}-positive terminals in the mPFC shows a rightward shift in input-output curves of APs in mPFC layer V pyramidal neurons. Two-way RM ANOVA. (**G** and **H**) Optogenetic activation of vHPC^{CaMK2A}-positive terminals in the mPFC decreases AP firing evoked by a ramp current in layer V mPFC pyramidal neurons. $^{**}P < 0.01$, paired *t* test. (**I** and **J**) In the presence of BIC (10 μM), optogenetic activation of vHPC^{CaMK2A}-positive terminals in the mPFC fails to decrease AP firing evoked by a ramp current in layer V mPFC pyramidal neurons. Paired *t* test. (**K**) Optogenetic activation of vHPC^{CaMK2A}-positive terminals evokes oEPSC and oIPSC in layer V mPFC pyramidal neurons, which can be completely blocked by application of TTX (1 μM), and only oEPSC was reinduced by 4-AP (100 μM) in the presence of TTX, indicating that the oEPSCs are elicited by direct synaptic connections between mPFC-projecting vHPC^{CaMK2A} neurons. (**L**) Both oEPSC and oIPSC are blocked by application of AMPA receptor antagonist CNQX (10 μM). (**M**) Schematic showing that mPFC inhibitory interneurons (IN) may mediate vHPC^{CaMK2A}-driven feed-forward inhibition to mPFC layer V pyramidal neurons (PN). Data are expressed as means ± SEM. Sample sizes are indicated in bars and parentheses.

vHPC-mPFC postsynaptic CRH^{+} neurons mediate vHPC-driven feed-forward inhibition to layer V pyramidal neurons

We next investigated the identities of mPFC inhibitory neurons modulating anxiodepressive-like behaviors. A subset of GABAergic neurons, CRH-positive GABAergic neurons, have been identified in the mPFC (*28*, *29*). Consistent with previous findings, RNAscope FISH revealed that approximately 23% of *vGat* mRNA-positive GABAergic neurons are colabeled with *Crh* mRNA-positive signals in the mPFC, and no colabeled signals of *vGlut1*$^{+}$ and *Crh*$^{+}$ were observed in the mPFC (Fig. 5A). This proportion was also confirmed in CRH-Cre::Ai14 mice (fig. S6A). To determine whether mPFC CRH^{+}

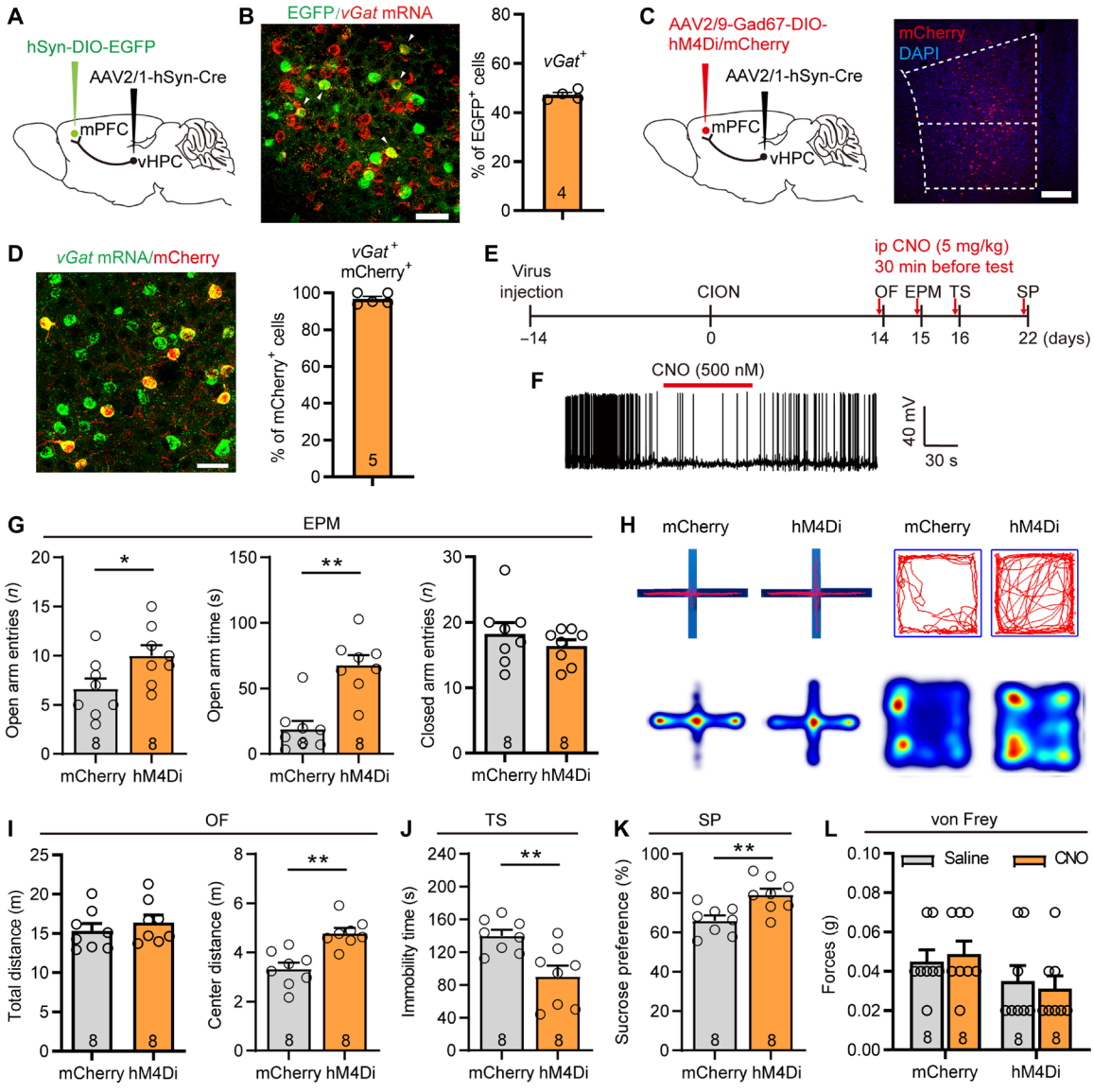

Fig. 4. The vHPC-mPFC^{GABA} projections contribute to CION-induced anxiodepressive behaviors. (**A**) Sagittal schematic showing specific infection of EGFP on mPFC postsynaptic neurons receiving projections from the vHPC. (**B**) RNAscope FISH showing colocalization and proportion of *vGat* mRNA with mPFC postsynaptic EGFP$^+$ neurons receiving projections from the vHPC. Scale bar, 50 μm. (**C**) Schematic and photomicrograph of coronal section showing specific infection of hM4Di or mCherry on mPFC postsynaptic Gad67$^+$ interneurons receiving projections from the vHPC. Scale bar, 200 μm. (**D**) RNAscope FISH showing colocalization and proportion of *vGat* mRNA with mPFC postsynaptic Gad67-mCherry$^+$ neurons receiving projections from the vHPC. Scale bar, 50 μm. (**E**) Schematic of the protocol in experiments (G) to (L). (**F**) Patch clamp recording in mPFC slice showing that APs are suppressed by bath CNO (500 nM) in mPFC postsynaptic Gad67$^+$ GABAergic neuron expressing hM4Di. (**G** to **K**) Chemogenetic inhibition of mPFC postsynaptic GABAergic neurons receiving projections from the vHPC effectively ameliorates CION-induced anxiodepressive-like behaviors in EPM [(G) and (H)], OF [(H) and (I)], TS (J), and SP (K) test. (H) Example track plots (top) and combined heatmap of two groups of animals (bottom) from mCherry- and hM4Di-injected mice in EPM (left) and OF (right) tests. *$P < 0.05$, **$P < 0.01$, two-tailed Student's *t* test. (**L**) Chemogenetic inhibition of mPFC postsynaptic GABAergic neurons receiving projections from the vHPC has no effect on CION-induced mechanical allodynia. Two-way ANOVA. Data are expressed as means ± SEM. Sample sizes are indicated in bars. See also figs. S3 to S5.

neurons receive direct projections from vHPC neurons, we injected AAV2/1-hsyn-Flpo virus into the vHPC and Flp-dependent AAV2/9-hEF1α-fDIO-EYFP into the mPFC of CRH-Cre::Ai14 mice. We detected over 30% of tdTomato-labeled mPFC CRH$^+$ neurons colocalized with EYFP (Fig. 5B), indicating that mPFC CRH$^+$ neurons receive axonal projections from vHPC neurons. Furthermore, we injected AAV-CaMK2A-ChR2 into the vHPC of CRH-Cre::Ai14 mice and then performed opto-electrophysiological recording and tested whether optogenetic activation of vHPC CaMK2A$^+$ presynaptic terminals in the mPFC is able to evoke EPSCs in mPFC CRH$^+$ neurons (Fig. 5C). Patch clamp recording showed that, with blue light stimulation of the vHPC^{CaMK2A} terminal in the mPFC, an oEPSC was evoked in 34 of 51 (66.7%) of recorded CRH$^+$ neurons (Fig. 5D). The recorded oEPSCs could be completely blocked by TTX and rescued

by TTX/4-AP, indicating that the oEPSCs were elicited by direct synaptic connections between vHPC^{CaMK2A} and mPFC^{CRH} neurons (Fig. 5E). Furthermore, optogenetic activation of vHPC^{CaMK2A} terminals in the mPFC resulted in c-Fos expression in more than 60% of CRH-positive neurons, indicating a functional connection between vHPC^{CaMK2A} and mPFC^{CRH} neurons (fig. S6, B and C).

We next showed an increased excitatory input of the vHPC^{CaMK2A}-mPFC^{CRH} pathway in CION mice. Optogenetic activation of vHPC CaMK2A$^+$ presynaptic terminals in the mPFC evoked a larger oEPSC in CRH$^+$ neurons of CION mice; the amplitude of oEPSCs induced by different intensities of blue light stimulation was robustly greater in CION mice than that of sham mice on day 14 (Fig. 5F). To confirm the presynaptic effects, we recorded oEPSCs evoked by paired pulse light stimulation of vHPC^{CaMK2A} terminals in mPFC slices. Within 50- to 150-ms intervals, paired-pulse ratios (PPRs) were reduced in CION mice as compared with controls (Fig. 5G). Because the PPR is inversely related to release probability, these results indicate that TN enhanced excitatory synaptic transmission from the vHPC^{CaMK2A} to mPFC^{CRH} by increasing presynaptic glutamate release. Furthermore, besides increased presynaptic inputs, CION also led to increased excitability of CRH$^+$ neurons, as indicated by a leftward shift in the input-output curve of APs evoked by step depolarizing current with a more hyperpolarized firing threshold in CION mice (Fig. 5, H and I, and fig. S6, D to I). Bath perfusion of the AMPA receptor antagonist CNQX (10 μM) and *N*-methyl-D-aspartate receptor antagonist D,L-2-amino-5-phosphonovaleric acid (50 μM) in mPFC slices from CION mice, a rightward shift in the input-output curve of APs evoked by step depolarizing current was observed in CRH$^+$ neurons (fig. S5, J and K), suggesting that the increase in excitatory inputs may be involved in the increase in excitability of CRH$^+$ neurons in TN mice. Moreover, cell-attach recordings of mPFC CRH$^+$ neurons showed that average spontaneous firing frequency was greatly increased after CION (Fig. 5J and fig. S6L).

We next investigated whether the vHPC-mPFC^{CRH} projections provided the inhibitory inputs onto layer V pyramidal neurons of the mPFC. To do this, we used the Cre-Flpo double enzyme system to generate mPFC postsynaptic CRH$^+$ neurons expressing ChR2 (Fig. 5K). Optogenetic activation of CRH$^+$ neurons expressing ChR2 evoked oIPSCs in layer V pyramidal neurons in mPFC slices, which could be blocked with the $GABA_A$ receptor inhibitor BIC (Fig. 5L). The oIPSCs were also blocked by TTX and rescued by 4-AP, indicating that the CRH$^+$ GABAergic neurons receiving vHPC projections mediated feed-forward inhibition to layer V pyramidal neurons (Fig. 5M).

vHPC-mPFC postsynaptic CRH$^+$ neurons contribute to CION-induced anxiodepressive behaviors

To determine the role of vHPC-mPFC^{CRH} projections in driving CION-induced anxiodepression, we used a Cre-enabled optogenetic inhibition system by injecting AAV2/1-FLEX-Flpo into the vHPC and Flp-dependent eNpHR (fDIO-eNpHR-EYFP) into the mPFC of CRH-Cre mice (Fig. 6A). By this way, we achieved selective inhibition of postsynaptic mPFC CRH$^+$ neurons receiving vHPC projections by yellow light stimulation. We then found that inhibition of mPFC CRH$^+$ neurons led to an attenuation of anti-anxiodepressive–like behaviors measured by the EPM, OF, and TS tests, without affecting mechanical hypersensitivity (Fig. 6, B to H). These results imply that the vHPC-mPFC^{CRH} pathway contributes to CION-induced anxiodepressive-like behaviors. To further confirm this, we inhibited mPFC CRH$^+$ neurons optogenetically with intra-mPFC injection of AAV-DIO-eNpHR-mCherry virus in CRH-Cre mice. The anti-anxiodepressive effect of inhibiting vHPC-mPFC^{CRH} postsynaptic CRH$^+$ neurons could be mimicked by optogenetic inhibition of mPFC CRH$^+$ neurons per se (fig. S7). These data indicate that mPFC CRH$^+$ neurons are necessary for the development of TN-induced anxiodepressive-like behaviors.

Considering CRH is coexpressed with vasoactive intestinal polypeptide (VIP) or somatostatin (SOM) but not parvalbumin in cortical neurons (*28*, *29*), we also examined the effects of inhibiting the vHPC-mPFC^{VIP} or vHPC-mPFC^{SOM} pathway on CION-induced anxiodepressive-like behaviors. Similar to inhibition of the vHPC-mPFC^{GABA} and vHPC-mPFC^{CRH} pathways, optogenetic inhibition of the vHPC-mPFC^{VIP} pathway, but not the vHPC-mPFC^{SOM} pathway, significantly attenuated CION-induced anxiodepressive-like behaviors (fig. S8). Thus, the VIP-expressing subset of mPFC CRH$^+$ neurons are crucial for TN to induce anxiodepressive-like behaviors.

CRH-CRHR1 signaling in the mPFC contributes to TN-induced anxiodepressive-like behaviors

We next examined whether the CRH-mediated signaling is crucial for driving anxiodepressive-like behaviors. We first observed an increase in *Crh* mRNA expression in mPFC *vGat*$^+$ inhibitory neurons by RNAscope FISH on day 14 after CION (fig. S9A). We then found that for two CRH receptors, CRHR1 rather than CRHR2 is expressed prominently in the mPFC (fig. S9B), especially in excitatory pyramidal neurons of the mPFC layer V (fig. S9, C and D). We next tested whether the CRH-CRHR1 signaling was involved in driving TN-induced anxiodepression. First, gain-of-function studies showed that activation of CRHR1 via injection of the CRHR1 agonist stressin-1 (200 ng/0.2 μl) bilaterally into the mPFC of naïve mice was sufficient to drive typical anxiodepressive-like behaviors, as indicated by less open arm time in the EPM test, more immobile time in the TS test, and less sucrose consumption in the SP test (Fig. 7, A to D). Second, we conducted loss-of-function studies and found that intra-mPFC injection of CRHR1 antagonist NBI27914 significantly improved CION-induced anxiodepressive-like behaviors (Fig. 7, E to I). Moreover, we used the Cre-Flpo double enzyme system to enabled vHPC-mPFC postsynaptic CRH$^+$ neurons expressing the Gq-coupled human muscarinic M3 designer (hM3D) receptor (Fig. 7, J and K). The efficacy of hM3Dq-mediated excitation was confirmed by patch clamp recordings in mPFC slices. AP firing was induced by CNO (500 nM) in mPFC CRH$^+$ neurons expressing hM3Dq (Fig. 7L). Chemogenetic activation of mPFC CRH$^+$ neurons receiving projections from the vHPC produced anxiodepressive-like behaviors, which could be blocked by the CRHR1 antagonist NBI27914 (Fig. 7, M to O).

Next, we determined whether activation of the CRHR1 signaling could modulate the activity of the layer V mPFC pyramidal neurons in response to the activation of mPFC^{CRH} neurons. In response to bath perfusion of the CRHR1 antagonist NBI27914 (5 μM) in mPFC slices from CION mice, layer V mPFC pyramidal neurons showed increased excitability and decreased amplitude of sIPSCs (Fig. 8, A to G, and fig. S9, F to H). We also examined the effect of CRH on the activity of layer V mPFC pyramidal neurons in naive mice. It was known that CRH/CRHR1 mainly exert their physiological functions by activating G protein–coupled receptor–associated cell signaling cascades (*30*). Upon ligand activation, signals are mainly coupled by Gαs, leading to increase in cyclic adenosine 3′,5′-monophosphate (cAMP) and protein kinase A (PKA) (*31*). Thus, activation of CRHR1 generally promotes neuronal excitability. However,

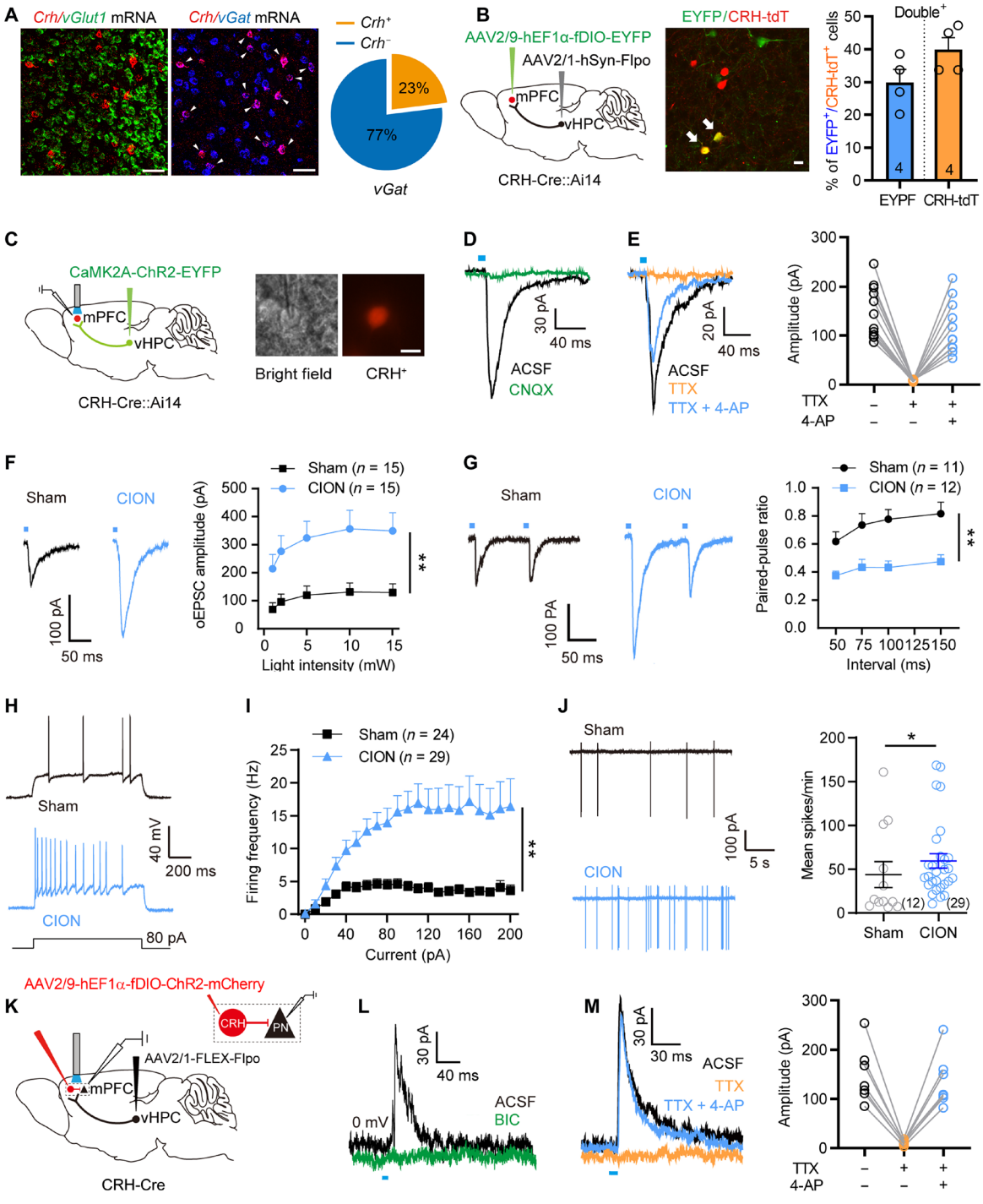

Fig. 5. TN enhances vHPC^{CaMK2A} excitatory inputs and the excitability of mPFC CRH$^+$ neurons. (**A**) RNAscope FISH showing colocalization and proportion of *vGlut1* or *vGat* mRNA with *Crf* mRNA in the mPFC. Scale bars, 50 μm. (**B**) Sagittal schematic and photomicrograph of coronal section showing mPFC postsynaptic CRH$^+$ neurons receiving projections from the vHPC. Scale bar, 20 μm. Histogram showing the proportion of CRH$^+$ neurons in the mPFC which receive input from the vHPC. (**C**) Sagittal schematic showing CaMK2A-ChR2 injection into the vHPC of CRH-Cre::Ai14 mice and mPFC slice image showing a recording electrode in a CRH$^+$ neuron. Scale bar, 20 μm. (**D** and **E**) Optogenetic activation of vHPC^{CaMK2A} inputs evokes oEPSCs in mPFC CRH$^+$ neurons, which can be completely blocked by application of CNQX (D) and TTX (E) and reinduced by 4-AP in the presence of TTX (E). (**F** and **G**) Optogenetic activation of vHPC^{CaMK2A} inputs induces an increased amplitude of oEPSCs (F) and a decreased paired-pulse ratio (PPR; G) in mPFC postsynaptic CRH$^+$ neurons from CION-14d mice. $^{**}P < 0.01$, two-way RM ANOVA. (**H** and **I**) CION increases firing frequency of APs evoked by depolarizing current steps in mPFC CRH$^+$ neurons on day 14. $^{**}P < 0.01$, two-way RM ANOVA. (**J**) CION increases spontaneous firing frequency in mPFC CRH$^+$ neurons by cell-attach recording. $^{*}P < 0.05$, two-tailed Student's *t* test. (**K**) Sagittal schematic showing the protocol of optogenetic manipulating mPFC postsynaptic CRH$^+$ neurons and patch clamp recording mPFC layer V pyramidal neurons. (**L** and **M**) Optogenetic activation of mPFC postsynaptic CRH$^+$ neurons evokes oIPSCs in mPFC layer V pyramidal neurons, which is completely blocked by application of BIC (L) or TTX, and 4-AP could rescue the oIPSCs in the presence of TTX (M). Data are expressed as means ± SEM. Sample sizes are indicated in bars and parentheses. See also fig. S6.

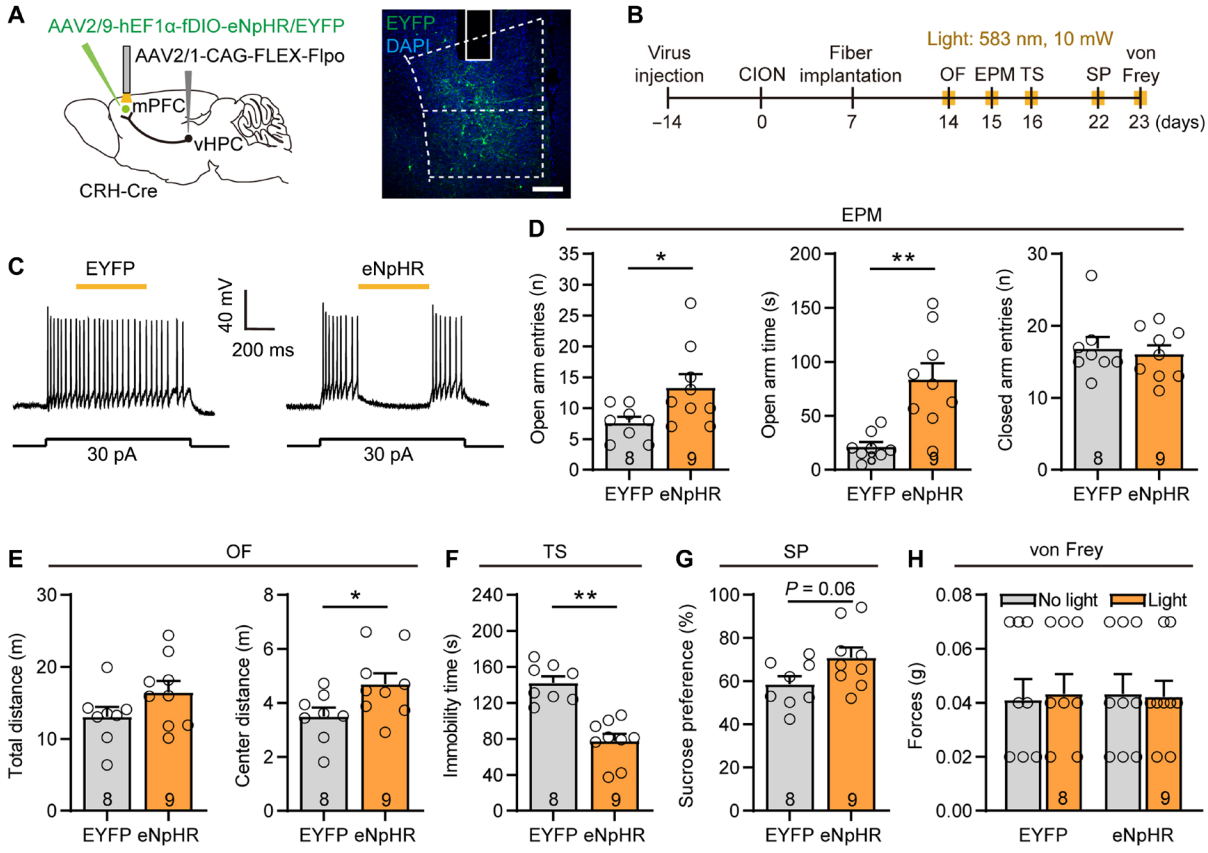

Fig. 6. Inhibition of vHPC-mPFC^{CRH} pathway and blockade CRHR1 improves CION-induced anxiodepressive behaviors. (**A**) Sagittal schematic and photomicrograph of coronal section showing specific infection of eNpHR or EYFP on mPFC postsynaptic CRH$^+$ neurons receiving projections from the vHPC in CRH-Cre mice. Scale bar, 200 μm. (**B**) Schematic of the protocol in experiments (D) to (H). (**C**) Patch clamp recording in mPFC slice showing that APs are suppressed by yellow light stimulation in mPFC postsynaptic CRH$^+$ neurons expressing eNpHR. (**D** to **G**) Optogenetic inhibition of mPFC postsynaptic CRH$^+$ neurons improves CION-induced anxiodepressive-like behaviors. *$P < 0.05$, **$P < 0.01$, two-tailed Student's t test. (**H**) Optogenetic inhibition of mPFC postsynaptic CRH$^+$ neurons does not affect CION-induced mechanical allodynia. Two-way ANOVA. Data are expressed as means ± SEM. Sample sizes are indicated in bars. See also figs. S7 and S8.

bath perfusion of CRF (200 nM) mimicked CION-induced deactivation of layer V mPFC pyramidal neurons, including reduced AP firing frequency, hyperpolarized RMP, and increased sIPSC amplitude (Fig. 8, H to N, and fig. S9, I to K). As a support, intra-mPFC injection of CRHR1 agonist stressin-1 (200 ng//0.2 μl) failed to increase c-Fos expression in layer V mPFC neurons (fig. S10, A and B). Furthermore, we examined the effect of blocking CRH-CRHR1 signaling on GABA-evoked currents in layer V mPFC pyramidal neurons. Puff application of GABA (100 μM) at 0 mV evoked an outward current, and application of CRF potentiated the GABA currents, which could be blocked by the CRHR1 antagonist NBI27914 (Fig. 8O). G protein inhibitor Guanosine-5'-O-(2-thiodiphosphate) trilithium salt [(GDP-β-S) 1 μM] in the intracellular solution completely prevented CRF-induced potentiation of the GABA current (Fig. 8P). In addition, oIPSCs of layer V pyramidal neurons evoked by optogenetic activating vHPC-mPFC postsynaptic CRH$^+$ neurons were partially attenuated by the CRHR1 antagonist NBI27914 (Fig. 8Q). These results suggest that CRH-CRHR1 signaling may regulate the inhibitory synaptic transmission of layer V mPFC pyramidal neurons by enhancing the function of the postsynaptic $GABA_A$ receptor. Behaviorally, we observed the effect of blocking $GABA_A$ receptors on CRH-mediated anxiodepressive-like behaviors. Chemogenetic activation of mPFC CRH$^+$ neurons receiving projections from the vHPC produced anxiodepressive-like behaviors, which could be blocked by the $GABA_A$ receptor antagonist BIC (3 ng/0.2 μl; fig. S10, C to H). These results suggest that both the CRH and GABA signaling in the mPFC contribute to CION-induced anxiodepression.

DISCUSSION

We identified a vHPC^{CaMK2A}-mPFC^{CRH} circuit involving the anxiodepressive consequences of neuropathic pain. The CRH-CRHR1 signaling operating within the vHPC^{CaMK2A}-mPFC^{CRH} circuit is required to induce anxidepressive-like consequences (Fig. 9).

Layer V pyramidal neurons provide the main integrated outputs of the mPFC (*32*), and persistent deactivation of layer V mPFC pyramidal neurons has been observed in rodent chronic pain models (*33*–*36*). Similarly, the activity of the dorsal lateral PFC (dlPFC) in humans (the homolog of rodent mPFC) is reduced in patients with persistent pain in rheumatoid arthritis (*37*) and ulcerative colitis (*38*). Stimulation of the dlPFC in humans and the mPFC in rats can effectively treat chronic pain and anxiodepressive behaviors (*39*, *40*). In this study, we have now provided insight into the mechanisms leading to inactivation of layer V pyramidal neurons in mice with chronic TN. In TN mice, sustained trigeminal pain leads to

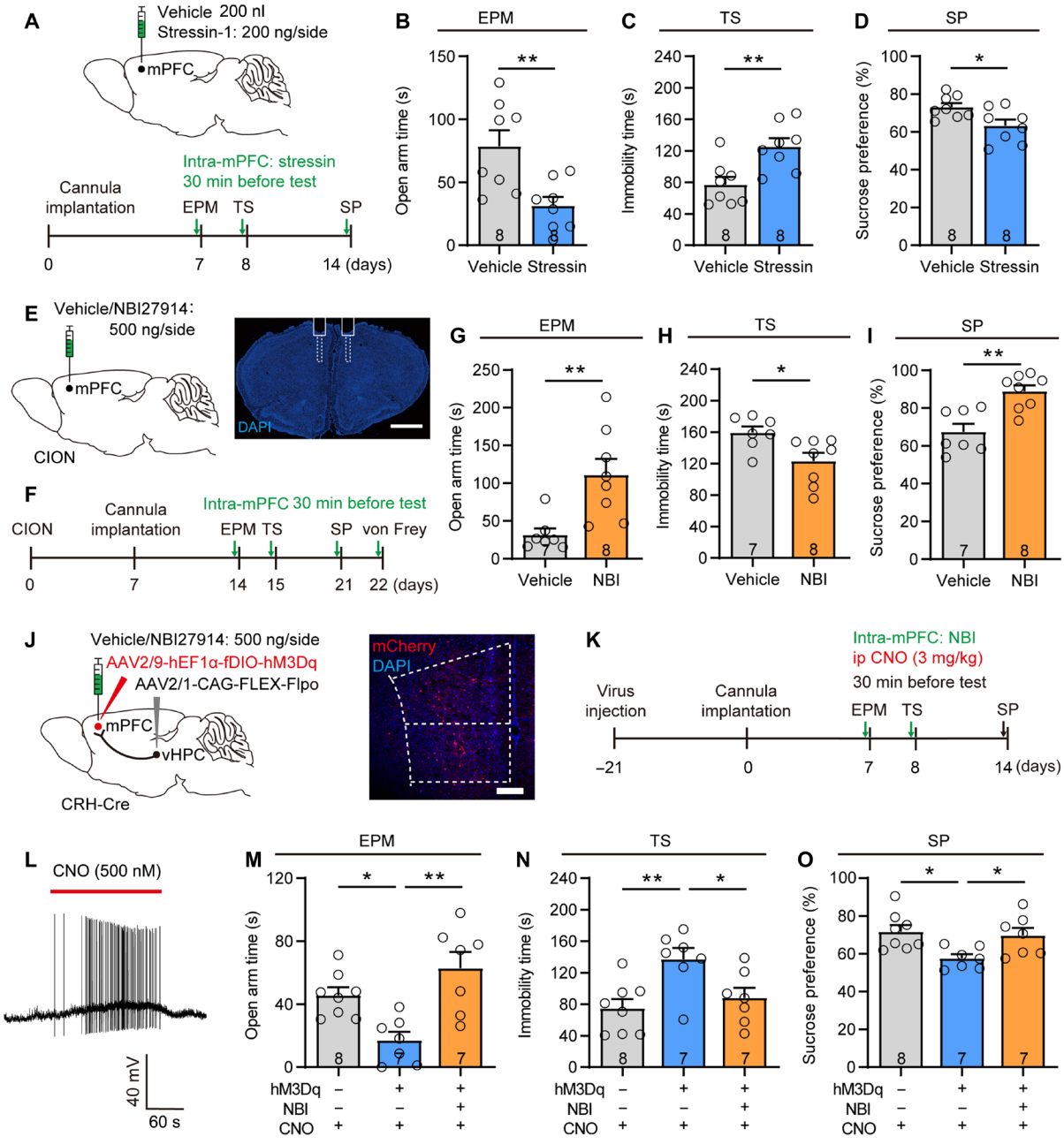

Fig. 7. Activation of CRH-CRHR1 signaling in the mPFC is sufficient to induce anxiodepressive-like behaviors. (**A**) Sagittal schematic of intra-mPFC injection and the protocol of experiments (B) to (D). (**B** to **D**) Intra-mPFC injection of CRHR1 agonist stressin-1 induces anxiodepressive-like behaviors in naive mice. $^{*}P < 0.05$, $^{**}P < 0.01$, two-tailed Student's *t* test. (**E**) Sagittal schematic and photomicrograph of coronal section showing the position of drug injection and cannula in the mPFC. Scale bar, 1 mm. (**F**) Schematic of the protocol in experiments (G) to (I). (**G** to **I**) Intra-mPFC injection of CRHR1 antagonist NBI27914 (NBI) significantly alleviates CION-induced anxiodepressive-like behaviors in EPM (G), TS (H), and SP (I) tests. $^{*}P < 0.05$, $^{**}P < 0.01$, two-tailed Student's *t* test. (**J**) Sagittal schematic and photomicrograph of coronal section showing specific infection of hM3Dq or mCherry on mPFC postsynaptic CRH^{+} neurons receiving projections from the vHPC and CRHR1 antagonist NBI27914 injection into the mPFC in CRH-Cre mice. Scale bar, 200 μm. (**K**) Schematic of the protocol in experiments (M) to (O). (**L**) In current clamp model, application of CNO (500 nM) evokes spontaneous APs in a mPFC postsynaptic CRH^{+} neuron expressing hM3Dq. (**M** to **O**) Chemogenetic activation of mPFC postsynaptic CRH^{+} neurons receiving projections from the vHPC produces anxiodepressive-like behaviors in naive mice, which is significantly improved by intra-mPFC injection of CRHR1 antagonist NBI27914 in EPM (M), TS (N), and SP (O) tests. $^{*}P < 0.05$, $^{**}P < 0.01$, one-way ANOVA followed by post hoc Dunn's test. Data are expressed as means ± SEM. Sample sizes are indicated in bars. See also fig. S9.

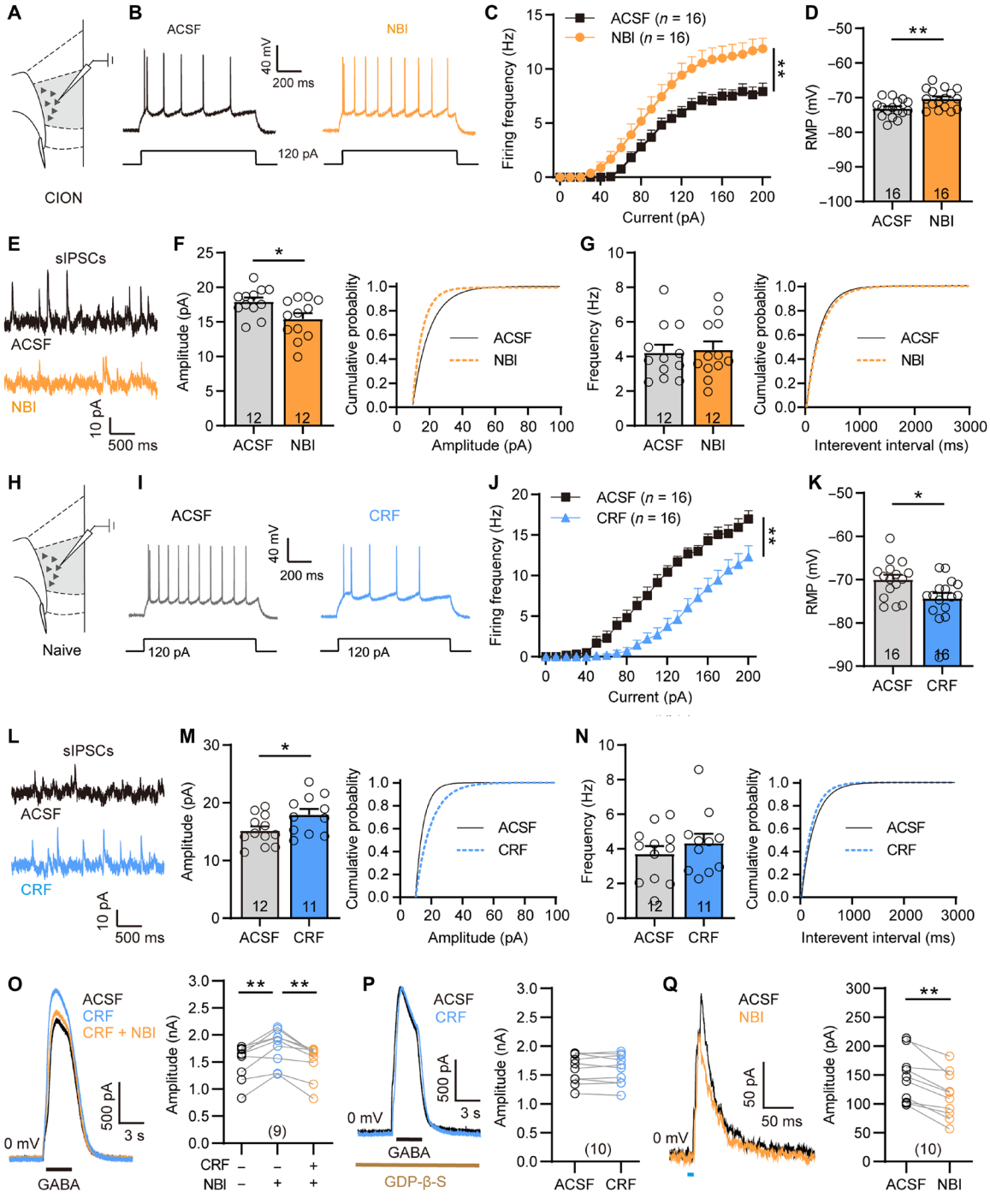

Fig. 8. CRH-CRHR1 signaling modulates the activity of layer V mPFC pyramidal neurons through postsynaptic $GABA_A$ receptor. (**A**) Schematic showing the location of the recorded neurons in mPFC layer V pyramidal neurons in CION-14d mice. (**B** and **C**) Bath application of CRHR1 antagonist NBI27914 (5 μM) increases firing frequency of APs evoked by depolarizing current steps in layer V mPFC pyramidal neurons from CION-14d mice. $^{**}P < 0.01$, two-way RM ANOVA. (**D**) The effect of CRHR1 antagonist NBI27914 on RMP of layer V mPFC pyramidal neurons from CION-14d mice. $^{**}P < 0.01$, two-tailed Student's *t* test. (**E** to **G**) Patch clamp recording of sIPSCs showing that CRHR1 antagonist NBI27914 decreases the amplitude of sIPSCs. $^{*}P < 0.05$, two-tailed Student's *t* test. (**H**) Schematic showing the location of the recorded neurons in layer V mPFC pyramidal neurons in naive mice. (**I** to **K**) Bath application of CRF (200 nM) mimics CION-induced inhibitory effects on AP firing and RMP of layer V mPFC pyramidal neuron. $^{**}P < 0.01$, two-way RM ANOVA for (J); $^{*}P < 0.05$, two-tailed Student's *t* test for (K). (**L** to **N**) Bath application of CRF (200 nM) significantly increases the amplitude of sIPSCs of layer V mPFC pyramidal neurons in naive mice. $^{*}P < 0.05$, two-tailed Student's *t* test. (**O**) Perfusion of CRF significantly enhances the amplitude of GABA currents in layer V mPFC pyramidal neurons, which is blocked by CRHR1 antagonist NBI27914. $^{**}P < 0.01$, paired *t* test. (**P**) GDP-β-S (1 μM) in the intracellular solution completely prevents CRF from increasing GABA currents. Paired *t* test. (**Q**) Optogenetic activation of mPFC postsynaptic CRH^+ neurons evokes oIPSCs in layer V mPFC pyramidal neurons, which is significantly attenuated by bath application of CRHR1 antagonist NBI27914. $^{**}P < 0.01$, paired *t* test. Data are expressed as means ± SEM. Sample sizes are indicated in bars and parentheses. See also figs. S9 and S10.

enhanced activity of CaMK2A$^+$ vHPC neurons, which in turn produced increased excitatory inputs to the CRH$^+$ subset of GABAergic neurons in the mPFC, causing a feed-forward inhibition of layer V mPFC pyramidal neurons. Notably, this enhanced feed-forward inhibition occurs after 14 days of TN, coinciding with the time window of the development of anxiodepressive-like consequences (*21*). Consistently, inactivation and activation of the vHPC^{CaMK2A}-mPFC^{CRH} circuits can sufficiently suppress and produce anxiodepressive-like consequences in TN and naïve mice, respectively. However, a study from Zhou's laboratory showed that inhibition or ablation of CRH neurons in the dorsal mPFC (dmPFC) facilitated social avoidance and depressive-like behaviors in a social defeat stress mouse model, while activation showed the opposite effect (*29*). This discrepancy implies the complexity of the CRH neuronal circuits and the specificity in etiology of depression. It has been implied that different etiologies of anxiety and depression (such as restraint stress and chronic pain) were encoded in different neurons and neural circuits (*41*, *42*). Thus, it is reasonable that mPFC^{CRH} neurons play different roles in different stress (social stress versus chronic pain) model animals. Alternatively, the discrepancy can be explained by the involvement of different mPFC subdivision in different behavioral functions. Subregions of the mPFC include the dorsal and ventral subdivisions, termed prelimbic (PL) and infralimbic (IL), respectively. Accumulating evidence has shown that PL and IL project very differently throughout the brain (*43*, *44*) and play different or even opposite roles in certain behavioral regulation (*22*, *45*). Because both PL-mPFC^{CRH} and IL-mPFC^{CRH} receiving projections from vHPC^{CaMK2A} neurons, we manipulated CRH$^+$ neurons in a broader region, including PL-mPFC and IL-mPFC. Differently, Chen *et al.*'s study (*29*) focused on dmPFC (PL-mPFC) subdivision, and their manipulation of CRH$^+$ neurons was limited to the dmPFC.

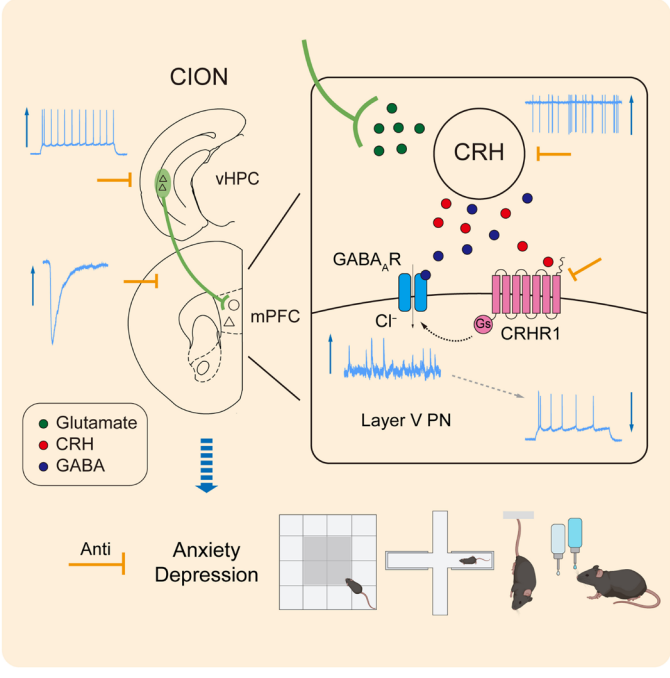

Fig. 9. A schematic showing that vHPC-mPFC circuit and CRH-CRHR1 signaling contribute to anxiodepressive consequences of TN. CION enhances excitatory activity of vHPC CaMK2A$^+$ pyramidal neurons and reinforces the excitatory inputs from vHPC to mPFC^{CRH} neurons. CRH-CRHR1 signaling may regulate excitatory/inhibitory activity of mPFC layer V pyramidal neurons via modulating GABA$_A$ receptor (GABA$_A$R), leading to anxiodepressive consequences of TN. Related to Discussion.

As chronic pain progresses, daily life activity such as food chewing (in terms of the TN model) could become a conditioned stimulus predicting the presence of an unconditioned outcome: the pain experience. To survive, animals have to eat, and accordingly, exaggerate pain becomes inevitable experience. This may explain why anxiety and depression develop much faster for this pain model in comparison with limb neuropathic pain models, for example, spared nerve injury or sciatic nerve injury model (*4*, *20*, *46*), and why TN causes so much emotional suffering and depression in humans (*47*, *48*). Previous studies demonstrated that vHPC excitatory neurons could regulate the activity of mPFC pyramidal neurons through GABAergic interneurons, gating fear extinction and relapse (*10*, *16*). Extinction deficits have been considered a mechanism for the persistence of pain and pain-related negative emotion (*18*). This may explain the involvement of the vHPC^{CaMK2A}-mPFC^{CRH} circuit in driving anxiety and depression in TN mice, which might result from pain-related emotional learning (e.g., pain-related fear, anxiety, and aversion) from the unconditioned persistent presence of pain or pain episodes evoked by unavoidable daily activity (*49*–*51*).

In addition, we found that CRH itself contributes to the inactivation of layer V mPFC output neurons and TN-induced anxiodepression through CRHR1. CRH is a 41–amino acid peptide that functions as a neuromodulator in the brain, regulating several behavioral stress responses (*30*, *52*, *53*). Besides its well-known action on the hypothalamic-pituitary-adrenal axis, CRH also acts in other extrahypothalamic brain regions, such as mPFC, increasing anxiety-like responses and executive dysfunction induced by stress (*31*, *54*). In postmortem levels, CRH immunoreactivity among depressed suicides is elevated in the PFC (*55*). In rodents, expression of *Crh* mRNA in the mPFC significantly increases after restraint stress (*54*, *56*). We observed that TN, as an unavoidable physical stress, also up-regulated *Crh* mRNA in mouse mPFC. Activation of CRHR1 in the mPFC directly produced anxiodepressive-like behaviors in naive mice. Blockade of CRHR1 in the mPFC significantly improved anxiodepressive-like behaviors caused by either TN or direct activation of vHPC-mPFC^{CRH} pathway. In particular, TN-induced inactivation of layer V mPFC pyramidal neurons was reversed by CRHR1 antagonist. These data suggest that endogenous CRH in the mPFC is required by anxiodepressive-like consequences of TN. We further showed that extracellular application of CRF in the mPFC mimicked TN-induced inactivation of layer V pyramidal neurons and anxiodepressive-like behaviors. Together, our results imply that both CRH$^+$ inhibitory neurons and their released CRF play crucial important roles in inactivating layer V mPFC output neurons and mediating anxiodepressive-like effect.

As mentioned above, CRH/CRHR1 signals are mainly coupled by Gαs, leading to neuronal excitability via increase in cAMP and PKA. However, our results showed that extracellular application of CRF inhibited neuronal excitability of layer V mPFC pyramidal neurons. One possible explanation is increased CRHR1 in GABAergic inhibitory neurons, which enhances the inhibitory input of layer V pyramidal neurons. What does not support this explanation is that our present results showed very few *Crhr1* mRNA in mPFC vGat-positive inhibitory neurons, with the vast majority in vGlut1-positive excitatory neurons. Alternatively, CRF may up-regulate the function of GABA receptors expressed in layer V pyramidal neurons through activating CRHR1-Gs-PKA signaling cascades. We

showed that CRF enhanced postsynaptic GABA currents of layer V mPFC pyramidal neurons; and this effect was prevented by pretreatment with CRHR1 antagonist or G protein inhibitor GDP-β-S. CRHR1 antagonist also suppressed sIPSC amplitude but not frequency of layer V mPFC pyramidal neurons in TN mice, suggesting a postsynaptic effect. Evidence that CRH augments GABAergic transmission through a postsynaptic action was also observed in the central amygdala (*57*) and bed nucleus of the stria terminalis (*58*). Moreover, in our observation, CRHR1 agonist did not increase c-Fos expression in mPFC neurons, implying the functional regulation of $GABA_A$ receptors by CRHR1. Also, blocked of $GABA_A$ receptors can prevent anxiodepressive-like behaviors caused by activation of vHPC-$mPFC^{CRH}$ pathway.

It is worth mentioning that our previous study showed that microglia and neuroinflammation in the ipsilateral but not the contralateral dHPC were involved in CION-induced anxiodepressive-like behaviors, suggesting an asymmetric role of dHPC (*21*). However, we did not find any difference in the anti-anxiodepressive effects produced by silent ipsilateral and contralateral vHPC neurons. As we know that the hippocampus is a heterogeneous structure with gradually segregated functional differences along the dorsal-ventral axis (*59*). The dHPC and vHPC exhibit different gene expression and have different connectivity with other cortical and subcortical structures (*60*–*62*), which leads to functional differences and often leads to opposite reactions to the same stimulus. For example, contrary to the present results of TN enhancing the excitability of vPHC excitatory neurons, chronic pain has been reported to reduce the excitability of dHPC pyramidal neurons and glutamate level in rodents (*63*, *64*). In addition, the activation of microglia and changes in neuronal activity induced by CION may also have quite different mechanisms. Thus, it is understandable that there is a difference in the laterality of the dHPC and vHPC.

Overall, we showed that inhibition of the $vHPC^{CaMK2A}$-$mPFC^{CRH}$ pathway or blockade of CRH-CRHR1 signaling in the mPFC effectively alleviated TN-induced anxiodepressive-like behaviors. Our studies will therefore help to develop therapeutic approaches for chronic pain–related anxiety and depression.

MATERIALS AND METHODS

Animals

Adult C57BL/6J mice (8 to 12 weeks old, 20 to 25 g; Shanghai Experimental Animal Center of Chinese Academy of Science) and transgenic strains CRH-ires-Cre (JAX#012704), Vip-ires-Cre (JAX#010908), SOM-ires-Cre (JAX#028864), Ai14 (JAX#007914), and R26R-EYFP (JAX#006148) were used in this study. All mice were maintained under standard housing conditions in a temperature (22° ± 1°C) and humidity controlled room with a 12-hour/12-hour light-dark cycle and food and water ad libitum. All experiments were approved by the Experimental Animal Ethics Committee of Shanghai Medical College and the Committee on the Use of Animal Experiments of Fudan University (permit SYXK2009-0082). The body weight and sex of animals were assigned to different treatment groups randomly. Behavioral testing, electrophysiological recording, and quantification of immunohistochemistry/FISH experiments were performed by researchers blinded to the treatments.

Chronic CION

The TN mouse model was established by chronic CION via an intraoral approach as described previously (*65*). Briefly, mice were anesthetized with sodium pentobarbital (50 mg/kg) by intraperitoneal injection, and the left infraorbital nerve was exposed proximal to the first molar along the left gingivocuccal margin. One ligature with 4-0 polyglycolic-co-lactic acid was tied loosely around the nerve. Sham-operated mice received nerve exposure without ligation. All surgical procedures were performed aseptically.

Virus stereotactic injection

Under sodium pentobarbital anesthesia, mice were fixed on a mouse stereotaxic apparatus (51725D, Stoelting, USA), and the skull plane was adjusted to ensure that the bregma and lambda were at a horizontal level. A small craniotomy hole was made using a dental drill, and a heating pad was used to maintain the body temperature at 37°C during anesthesia. A volume of 200 to 300 nl of virus (depending on the expression strength and viral titer) was injected through a glass microelectrode connected to a microinjection pump (Nanoliter 2010 injector, World Precision Instruments Inc., USA) at a rate of 30 nl/min. The stereotaxic coordinates for the vHPC were 3.2 mm anteroposterior (AP), ±3.7 mm mediolateral (ML), and −3.5 mm dorsoventral (DV); coordinates for the mPFC were +1.75 mm AP, ±0.4 mm ML, and −2.45 mm DV. At the end of the infusion, the glass pipette remained in the injection place for 10 min to avoid virus overflow. AAV details are shown in table S1. AAV expression was permitted for at least 3 weeks before the experiments; mice with off-target mCherry or EGFP localization were excluded from the analysis.

Cannula infusion

Mice were anesthetized with sodium pentobarbital and a stainless steel guide cannula (62028, RWD Life Science, Shenzhen, China) with a stainless steel stylet plug (62128, RWD) was implanted above the injection site in the mPFC. Dental cement and biocompatible adhesive were used to fix the cannula. Mice were allowed to recover for 1 week before behavior tests. Microinjection was performed through an injector cannula (62228, RWD), which protrudes 1.3 mm beyond the guide cannula to reach the site of mPFC. CRHR1 antagonist NBI27914 was dissolved in sesame oil (in vivo) or ethanol (in vitro). CRF, CRHR1 agonist stressin-1, and $GABA_A$ antagonist BIC were dissolved in normal saline. The chemical details are shown in table S1. A total of 200 nl of vehicle or drugs was injected per side at the rate of 100 nl/min. The injector cannula was held for 2 min before withdrawal to minimize drug spread along the injection track. Behavior tests were conducted after 30 min.

Behavior assessment

von Frey test

Mice were handled and habituated in the experimenter's hand for 10 min, for at least 3 days before testing. Mechanical sensitivity was determined using a series of von Frey filaments with increasing forces (0.02 to 2 g) applied to skin within the infraorbital territory, near the center of the vibrissa pads. A brisk or active withdrawal of the head from the filament was considered a response. Each filament was applied 10 times at 10-s intervals, and the lowest force in grams that evoked a positive withdrawal response in >50% of the 10 consecutive stimuli was defined as the withdrawal threshold.

Open field

The open field test consisted of an open box (length by width by height: 40 cm by 40 cm by 30 cm) and a data acquisition and analysis system. The observation area was divided into the angle zone (10 cm by 10 cm at the four corners) and the center of the area (20 cm by 20 cm). Mice were gently placed into the center of the arena at the beginning and allowed to explore freely for 5 min. Movement of the animals was recorded with a digital camera over the chamber. Video tracking software (Ethovision XT v11.5, Noldus BV) was used to analyze the distance traveled and time spent in each area.

Elevated plus maze

The EPM device consisted of two closed arms (length by width: 30 cm by 6 cm), two open arms (length by width: 30 cm by 6 cm) and a central platform (length by width: 6 cm by 6 cm) elevated 50 cm above the floor. The two closed arms were enclosed with 20-cm-high walls crossing with two open arms. Mice were gently placed in the central platform of the maze facing an open arm and were allowed to explore freely for 5 min. Movement of the animals in the maze was recorded with a digital camera over the maze. Both open/closed arm entries and open arm time were analyzed with video tracking software (Ethovision XT v11.5, Noldus BV).

Tail suspension

The TS box was made of polyethylene with the dimensions 30 cm by 30 cm by 30 cm. The mice were suspended in the middle of the box with the tape at 0.1 cm proximal to the tail tip, and the distance between the mouse's nose and the box floor was approximately 2 cm in the rest state. Mice activity was recorded with a digital camera for 6 min, and the immobility time in the last 4 min was counted.

Sucrose preference

The SP test was conducted as described previously (Sheng HY, JCI insight, 2020). The experimental procedure consisted of 6 days. On days 1 to 3 (from 17:00 on the first day to 17:00 on the third day), the mice were kept in a home cage with two bottles, one containing regular water and the other containing 1% fresh sucrose solution, to adapt for 48 hours. On days 3 to 4 (from 17:00 on the third day to 17:00 on the fourth day), the mice were placed in a black polyethylene apparatus (length by width by height: 50 cm by 24 cm by 13 cm) with a transparent polyethylene cover to adapt to the SP test apparatus for 24 hours. Each mouse was provided with two tubes (1% sucrose solution and regular water) in each chamber. On days 4 to 5, baseline measurements were determined for 12 hours (from 21:00 on the fourth day to 9:00 on the fifth day) in the SP test apparatus. After the baseline test, mice were deprived of food and water for 12 hours (from 9:00 to 21:00 on the fifth day) in home cages and then moved to the SP test apparatus for 12 hours (from 21:00 on the fifth day to 9:00 on the sixth day) to measure the SP rate. During this experiment, positions of the water and sucrose were changed every day. The SP rate was determined as follows: (sucrose consumption/total consumption) × 100%.

Optogenetic manipulation

Two weeks after injection of optogenetic viruses, optical fibers (Ø200-μm core, 0.37 numerical aperture; Newdoon Technology Co. Ltd., Hangzhou, China) were implanted 0.2 mm above the virus injection site under anesthesia. Mice were allowed to recover for 1 week. Before optogenetic stimulation, the laser source was adjusted to the proper intensity and connected to the implanted optical fiber through a fiber cable. The EPM, OF, and TS tests were performed with yellow light stimulation (538 nm, 10 mW, continuous). In SP test, light stimulation was applied for 10 min before the test.

Chemogenetic manipulation

For chemogenetic inhibition, the designed CNO (5 mg/kg in 0.1 ml, ip) was administered 30 min before behavioral tests. For chemogenetic activation, CNO (3 mg/kg, ip) was injected 30 min before behavioral tests. For pharmacological and chemogenetic manipulation, CNO (3 mg/kg, ip) was injected immediately after NBI27914 (500 ng) or BIC (3 ng) intracerebral injection.

Slice preparation and electrophysiological recording

Mice were deeply anesthetized and transcardially perfused with ice-cold cutting solution containing 92 mM *N*-methyl-D-glucamine, 2.5 mM KCl, 1.2 mM NaH_2PO_4, 20 mM Hepes, 30 mM $NaHCO_3$, 25 mM glucose, 5 mM Na ascorbate, 3 mM Na pyruvate, 2 mM thiourea, 10 mM $MgSO_4$, and 0.5 mM $CaCl_2$ (pH 7.3, 300 to 310 mOsm/liter). The brains were immediately removed and submerged in pre-oxygenated (95% O_2, 5% CO_2, v/v) cold cutting solution. Slices (300 μm) containing the vHPC or mPFC were cut using a vibrating microtome (VT1200S, Leica, Germany) and transferred to an oxygenated chamber filled with recording artificial cerebrospinal fluid (recording ACSF) containing 119 mM NaCl, 2.3 mM KCl, 1 mM NaH_2PO_4, 26.2 mM $NaHCO_3$, 12 mM glucose, 1.3 mM $MgSO_4$, and 2.5 mM $CaCl_2$ (pH 7.3 when carbogenated with 95% O_2 and 5% CO_2, 300 to 310 mOsm/liter) for 30 min at 32°C. The incubated brain slices were transferred to the recording chamber and continuously perfused with circulated well-oxygenated ACSF at a rate of 2 to 3 ml/min at room temperature. A charge-coupled device imaging system was used to find the vHPC CA1 area or mPFC using the IR-DIC mode with a low-power lens (×10) in an Olympus BX51WI upright microscope; a high-power lens (×60) was used to find the target neurons.

Whole-cell patch clamp recordings were performed with Axon 700B amplifier with a Digidata 1550B digitizer (Molecular Devices, USA). Patch pipettes (3 to 8 megohm) were made of borosilicate glass on a micropipette puller (P-1000, Sutter Instruments, Novato, CA, USA). The signals were low-pass–filtered at 2 kHz, digitized at 10 kHz, and analyzed with Clampfit 10.6 software (Molecular Devices). If the series resistance changed more than 20% during the recording, the recording was terminated. The current-evoked APs were recorded in current-clamp mode ($I = 0$ pA) and injected current steps from −50 to 200 pA in 10-pA steps. The electrodes were filled with K-gluconate internal solution containing 125 mM K-gluconate, 15 mM KCl, 0.5 mM EGTA, 10 mM Hepes, 10 mM phosphocreatine, 2 mM Mg–adenosine triphosphate (ATP), and 0.5 mM Na–guanosine triphosphate (GTP) (pH 7.3, 290 to 300 mOsm/liter).

The spontaneous firing activity was recorded in the cell-attached voltage-clamp mode. The pipette was filled with recording ACSF. The liquid junction potential was approximately zero. While approaching the neuron, positive pressure was applied to the patch electrode. By applying slight suction to the electrode, a seal (10 to 100 megohm) was created between the cell membrane and the recording pipette. Spontaneous firing activity was then recorded for 10 min and analyzed 5 min after stabilization.

For sEPSC and sIPSC recordings, electrodes were filled with Cs-methanesulfonate internal solution containing 127.5 mM Cs-methanesulfonate, 7.5 mM CsCl, 2.5 mM $MgCl_2{\cdot}6H_2O$, 0.6 mM EGTA, 10 mM Hepes, 10 mM phosphocreatine, 4 mM Na-ATP, and 0.4 mM Na-GTP (pH 7.3, 290 to 300 mOsm/liter). After establishing the whole-cell configuration, neurons were held at −70 and 0 mV to record sEPSCs and sIPSCs, respectively. Bath application of AMPA receptor blocker CNQX (10 μM) or $GABA_A$ receptor blocker BIC (10 μM) blocked the sEPSCs or sIPSCs, respectively. Continuous bath perfusion of drugs or ACSF (control) is performed during the recording. Different slices from the same animal were randomly assigned to control and drug-treated groups. In general, one to two cells were recorded in each slice of the drug-treated group. Data were sampled at 10 kHz, filtered at 2 kHz, and analyzed with the Mini Analysis Program (Synaptosoft).

For light-evoked excitatory postsynaptic currents (oEPSCs) and inhibitory postsynaptic currents (oIPSCs) recordings, optical stimulation (470 nm, light intensity 1 to 15 mW, 10 ms) was delivered by a light-emitting diode (LED; X-cite 110, USA), which was connected to the programmable pulse stimulator (Master-9, A.M.P. Instruments, Israel). oEPSCs or oIPSCs were recorded in voltage clamp mode (holding potential, −70 mV for oEPSCs and 0 mV for oIPSCs) with Cs-methanesulfonate internal solution. To record $vHPC^{CaMK2A}$-$mPFC^{CRH}$ synaptic transmission, light was delivered to $vHPC^{CaMK2A}$-positive terminals expressing ChR2 in the mPFC of CRH-Cre::Ai14 mice. To analyze the PPR, paired optical stimuli (470 nm, 5 mW, 10 ms, interpulse 50, 75, 100, and 150 ms) were applied, and the oEPSC2/oEPSC1 ratio was calculated. To record the synaptic transmission between mPFC CRH^+ neurons and layer V mPFC pyramidal neurons, light was delivered to mPFC CRH^+ neurons expressing ChR2 of CRH-Cre mice. To test whether the postsynaptic currents recorded in mPFC neurons were elicited by direct synaptic connections, 1 μM TTX and 100 μM 4-AP were added to ACSF. To obtain the GABA currents, the membrane potential was held at 0 mV, puffing GABA (100 μM) for 3 s.

Fiber photometry

AAV-CaMK2A-GCaMP6s virus was injected into the vHPC as described above, and optical fiber (Ø200-μm core) was implanted after 3 weeks. In vivo recording of vHPC Ca^{2+} activity was conducted after 1 week using a fiber photometry system (FPS-MC-LED, Thinker Tech). For assessment of vHPC neuronal activity in response to EPM exposure, mice were placed in the EPM, and movement of mice in the EPM and the Ca^{2+} signal of vHPC neurons were recorded simultaneously. Calcium-dependent fluorescent signals were recorded in GCaMP6s-expressing vHPC neurons using a 470-nm laser. The laser power at the tip of the optical fiber was adjusted to 30 μW to decrease laser bleaching. The moment when the mouse entered the open arm from the closed arm was defined as onset of the event. The baseline was the average Ca^{2+} transient 2 s before onset of the event. Z score ($\Delta F/\sigma F$) of the fluorescence change and area under the curve of changes in transient Ca^{2+} corresponding to events were analyzed. The heatmap and averaged Ca^{2+} traces were plotted using a MATLAB tool package.

Immunohistochemistry

Mice were deeply anesthetized and transcardially perfused with 0.9% saline followed by precold 4% paraformaldehyde (PFA) in 0.1 M phosphate buffer (PB) (pH 7.4). The brain was removed, postfixed in 4% PFA for an additional 4 to 8 hours at 4°C, and dehydrated with a sucrose gradient (10 to 30%) in PB at 4°C. Fixed frozen tissues were sectioned (30 μm) on a cryostat microtome (CM 1950, Leica, Germany). Sections were blocked with 10% normal donkey serum with 0.3% Triton X-100 in 0.01 M phosphate-buffered saline (PBS) for 2 hours at room temperature and incubated overnight at 4°C with chicken anti-GFP (1:1000, Aves labs), rabbit anti–red fluorescent protein (1:1000, Rockland), and rabbit anti c-Fos (1:2000, abcam) primary antibodies. After rinsing with PBS, sections were then incubated for 2 hours at room temperature with corresponding Alexa Fluor 488/546/647–conjugated secondary antibodies (1:500, Invitrogen) or 4′,6-diamidino-2-phenylindole (1:10,000, Invitrogen). The antibody details are shown in table S1. The stained sections were observed and analyzed with a confocal laser-scanning microscope (FV1000, Olympus, Japan).

Fluorescence in situ hybridization

FISH was performed using the RNAscope system [Advanced Cell Diagnostics (ACD)] according to the manufacturer's instructions. Sections were pretreated with hydrogen peroxide, target retrieval reagents, and protease III and then treated for 2 hours with targeted mRNA probes: *vGlut1* (ACDBio, 416631), *vGat* (ACDBio, 319191), *Crh* (ACDBio, 316091), *Crhr1* (ACDBio, 418011), and *Crhr2* (ACDBio, 423201), followed by AMP1, AMP2, and AMP3 successively for 15 to 30 min. The sections were further incubated in horseradish peroxidase-channel1/2/3 (HRP-C1/2/3) for 15 min and Opal 520/570/690 (1:1500, PerkinElmer) for 30 min to fluorescently label the probe. Finally, HRP blocker was added for 15 min after fluorescent labeling of each channel. All hybridization and incubation steps were performed at 40°C in the hybridization oven; moisture was maintained with the use of a wet box. Immunohistochemical staining was continued after these procedures.

Quantification of c-Fos immunostaining

To quantify the influence of activation of the vHPC-mPFC pathway on c-Fos expression in mPFC $vGat^+$ and CRH^+ neurons, eight vGat-Cre and eight CRH-Cre::R26R-EYFP mice were divided into two groups. vGat-Cre mice received mPFC injection of DIO-mCherry and vHPC injection of AAV-CaMK2A-ChR2 ($n = 4$) or AAV-CaMK2A-EYFP ($n = 4$); CRH-Cre::R26R-EYFP mice received vHPC injection of AAV-CaMK2A-ChR2 ($n = 4$) or AAV-CaMK2A-mCherry ($n = 4$). An optical fiber was implanted in the mPFC. Before transcardiac perfusion, each mouse was placed in the test environment alone for at least 3 hours to eliminate background signal. Then, blue light stimulation (473 nm, 5 mW, 10 ms, 20 Hz for 10 min) was delivered. After 90 min, the mice were anesthetized and perfused, and c-Fos immunohistochemistry staining was performed. In each mouse, the number of vGat-mCherry– or CRH-EYFP–labeled cells and c-Fos/vGat-mCherry or c-Fos/CRH-EYFP double-labeled cells was counted from four to six randomly selected equivalent areas of the mPFC. The percentage of c-Fos/vGat-mCherry or c-Fos/CRH-EYFP double-labeled mPFC cells in vGat-mCherry– or CRH-EYFP–labeled cells was calculated for four animals in each group.

Statistical analysis

Data are presented as mean ± SEM. Data from different groups were verified for normality and homogeneity of variance using

Shapiro-Wilk and Brown-Forsythe tests before analysis, where no data were transformed. No data were excluded from statistical analysis due to outlier status. Electrophysiological recording, FISH signals, and behavioral data were analyzed using the paired *t* test, Student's *t* test, or Mann-Whitney *U* test (nonparametric data) when comparing two groups or one-way analysis of variance (ANOVA) followed by post hoc Sidak or Dunn's test or two-way ANOVA followed by post hoc Sidak test or Kruskal-Wallis *H* test (nonparametric data) when comparing more than two groups. All analyses were two-tailed, and a *P* value less than 0.05 ($P < 0.05$) was considered statistically significant. Statistical analyses were performed using GraphPad Prism 8.0 software.

Supplementary Materials

This PDF file includes:

Figs. S1 to S10
Table S1
Legends for data files S1 and S2

Other Supplementary Material for this manuscript includes the following:

Data files S1 and S2

REFERENCES AND NOTES

1. B. Stubbs, D. Vancampfort, N. Veronese, T. Thompson, M. Fornaro, P. Schofield, M. Solmi, J. Mugisha, A. F. Carvalho, A. Koyanagi, Depression and pain: Primary data and meta-analysis among 237 952 people across 47 low- and middle-income countries. *Psychol. Med.* **47**, 2906–2917 (2017).
2. M. J. Bair, R. L. Robinson, W. Katon, K. Kroenke, Depression and pain comorbidity: A literature review. *Arch. Intern. Med.* **163**, 2433–2445 (2003).
3. M. Llorca-Torralba, C. Camarena-Delgado, I. Suarez-Pereira, L. Bravo, P. Mariscal, J. A. Garcia-Partida, C. Lopez-Martin, H. Wei, A. Pertovaara, J. A. Mico, E. Berrocoso, Pain and depression comorbidity causes asymmetric plasticity in the locus coeruleus neurons. *Brain* **145**, 154–167 (2022).
4. W. Zhou, Y. Jin, Q. Meng, X. Zhu, T. Bai, Y. Tian, Y. Mao, L. Wang, W. Xie, H. Zhong, N. Zhang, M. H. Luo, W. Tao, H. Wang, J. Li, J. Li, B. S. Qiu, J. N. Zhou, X. Li, H. Xu, K. Wang, X. Zhang, Y. Liu, G. Richter-Levin, L. Xu, Z. Zhang, A neural circuit for comorbid depressive symptoms in chronic pain. *Nat. Neurosci.* **22**, 1649–1658 (2019).
5. C. Y. Saab, Pain-related changes in the brain: Diagnostic and therapeutic potentials. *Trends Neurosci.* **35**, 629–637 (2012).
6. R. C. Bagot, E. M. Parise, C. J. Pena, H. X. Zhang, I. Maze, D. Chaudhury, B. Persaud, R. Cachope, C. A. Bolanos-Guzman, J. F. Cheer, K. Deisseroth, M. H. Han, E. J. Nestler, Ventral hippocampal afferents to the nucleus accumbens regulate susceptibility to depression. *Nat. Commun.* **6**, 7062 (2015).
7. E. Vachon-Presseau, P. Tetreault, B. Petre, L. Huang, S. E. Berger, S. Torbey, A. T. Baria, A. R. Mansour, J. A. Hashmi, J. W. Griffith, E. Comasco, T. J. Schnitzer, M. N. Baliki, A. V. Apkarian, Corticolimbic anatomical characteristics predetermine risk for chronic pain. *Brain* **139**, 1958–1970 (2016).
8. W. Cheng, E. T. Rolls, J. Qiu, X. Xie, D. Wei, C. C. Huang, A. C. Yang, S. J. Tsai, Q. Li, J. Meng, C. P. Lin, P. Xie, J. Feng, Increased functional connectivity of the posterior cingulate cortex with the lateral orbitofrontal cortex in depression. *Transl. Psychiatry* **8**, 90 (2018).
9. E. L. Belleau, M. T. Treadway, D. A. Pizzagalli, The impact of stress and major depressive disorder on hippocampal and medial prefrontal cortex morphology. *Biol. Psychiatry* **85**, 443–453 (2019).
10. F. Sotres-Bayon, D. Sierra-Mercado, E. Pardilla-Delgado, G. J. Quirk, Gating of fear in prelimbic cortex by hippocampal and amygdala inputs. *Neuron* **76**, 804–812 (2012).
11. A. Adhikari, M. A. Topiwala, J. A. Gordon, Synchronized activity between the ventral hippocampus and the medial prefrontal cortex during anxiety. *Neuron* **65**, 257–269 (2010).
12. N. Padilla-Coreano, S. S. Bolkan, G. M. Pierce, D. R. Blackman, W. D. Hardin, A. L. Garcia-Garcia, T. J. Spellman, J. A. Gordon, Direct ventral hippocampal-prefrontal input is required for anxiety-related neural activity and behavior. *Neuron* **89**, 857–866 (2016).
13. L. Ma, L. Yue, Y. Zhang, Y. Wang, B. Han, S. Cui, F. Y. Liu, Y. Wan, M. Yi, Spontaneous pain disrupts ventral hippocampal CA1-Infralimbic cortex connectivity and modulates pain progression in rats with peripheral inflammation. *Cell Rep.* **29**, 1579–1593.e6 (2019).
14. C. J. Kelly, M. Martina, Circuit-selective properties of glutamatergic inputs to the rat prelimbic cortex and their alterations in neuropathic pain. *Brain Struct. Funct.* **223**, 2627–2639 (2018).
15. M. L. Phillips, H. A. Robinson, L. Pozzo-Miller, Ventral hippocampal projections to the medial prefrontal cortex regulate social memory. *eLife* **8**, e44182 (2019).
16. R. Marek, J. Jin, T. D. Goode, T. F. Giustino, Q. Wang, G. M. Acca, R. Holehonnur, J. E. Ploski, P. J. Fitzgerald, T. Lynagh, J. W. Lynch, S. Maren, P. Sah, Hippocampus-driven feed-forward inhibition of the prefrontal cortex mediates relapse of extinguished fear. *Nat. Neurosci.* **21**, 384–392 (2018).
17. Q. Wang, Q. Wang, X. L. Song, Q. Jiang, Y. J. Wu, Y. Li, T. F. Yuan, S. Zhang, N. J. Xu, M. X. Zhu, W. G. Li, T. L. Xu, Fear extinction requires ASIC1a-dependent regulation of hippocampal-prefrontal correlates. *Sci. Adv.* **4**, eaau3075 (2018).
18. A. V. Apkarian, M. N. Baliki, P. Y. Geha, Towards a theory of chronic pain. *Prog. Neurobiol.* **87**, 81–97 (2009).
19. I. Yalcin, Y. Bohren, E. Waltisperger, D. Sage-Ciocca, J. C. Yin, M. J. Freund-Mercier, M. Barrot, A time-dependent history of mood disorders in a murine model of neuropathic pain. *Biol. Psychiatry* **70**, 946–953 (2011).
20. J. Sellmeijer, V. Mathis, S. Hugel, X. H. Li, Q. Song, Q. Y. Chen, F. Barthas, P. E. Lutz, M. Karatas, A. Luthi, P. Veinante, A. Aertsen, M. Barrot, M. Zhuo, I. Yalcin, Hyperactivity of anterior cingulate cortex areas 24a/24b drives chronic pain-induced anxiodepressive-like consequences. *J. Neurosci.* **38**, 3102–3115 (2018).
21. L. Q. Chen, X. J. Lv, Q. H. Guo, S. S. Lv, N. Lv, W. D. Xu, J. Yu, Y. Q. Zhang, Asymmetric activation of microglia in the hippocampus drives anxiodepressive consequences of trigeminal neuralgia in rodents. *Br. J. Pharmacol.* **180**, 1090–1113 (2023).
22. M. Fuchikami, A. Thomas, R. Liu, E. S. Wohleb, B. B. Land, R. J. DiLeone, G. K. Aghajanian, R. S. Duman, Optogenetic stimulation of infralimbic PFC reproduces ketamine's rapid and sustained antidepressant actions. *Proc. Natl. Acad. Sci. U.S.A.* **112**, 8106–8111 (2015).
23. C. E. Page, L. Coutellier, Prefrontal excitatory/inhibitory balance in stress and emotional disorders: Evidence for over-inhibition. *Neurosci. Biobehav. Rev.* **105**, 39–51 (2019).
24. C. J. Kelly, M. Huang, H. Meltzer, M. Martina, Reduced glutamatergic currents and dendritic branching of layer 5 pyramidal cells contribute to medial prefrontal cortex deactivation in a rat model of neuropathic pain. *Front. Cell. Neurosci.* **10**, 133 (2016).
25. F. R. Carreno, J. J. Donegan, A. M. Boley, A. Shah, M. DeGuzman, A. Frazer, D. J. Lodge, Activation of a ventral hippocampus-medial prefrontal cortex pathway is both necessary and sufficient for an antidepressant response to ketamine. *Mol. Psychiatry* **21**, 1298–1308 (2016).
26. B. R. Rost, J. Wietek, O. Yizhar, D. Schmitz, Optogenetics at the presynapse. *Nat. Neurosci.* **25**, 984–998 (2022).
27. B. Zingg, X. L. Chou, Z. G. Zhang, L. Mesik, F. Liang, H. W. Tao, L. I. Zhang, AAV-Mediated anterograde transsynaptic tagging: Mapping corticocollicular input-defined neural pathways for defense behaviors. *Neuron* **93**, 33–47 (2017).
28. Y. Kubota, N. Shigematsu, F. Karube, A. Sekigawa, S. Kato, N. Yamaguchi, Y. Hirai, M. Morishima, Y. Kawaguchi, Selective coexpression of multiple chemical markers defines discrete populations of neocortical GABAergic neurons. *Cereb. Cortex* **21**, 1803–1817 (2011).
29. P. Chen, S. Lou, Z. H. Huang, Z. Wang, Q. H. Shan, Y. Wang, Y. Yang, X. Li, H. Gong, Y. Jin, Z. Zhang, J. N. Zhou, Prefrontal cortex corticotropin-releasing factor neurons control behavioral style selection under challenging situations. *Neuron* **106**, 301–315.e7 (2020).
30. J. M. Deussing, A. Chen, The corticotropin-releasing factor family: Physiology of the stress response. *Physiol. Rev.* **98**, 2225–2286 (2018).
31. T. T. Miguel, K. S. Gomes, R. L. Nunes-de-Souza, Tonic modulation of anxiety-like behavior by corticotropin-releasing factor (CRF) type 1 receptor (CRF1) within the medial prefrontal cortex (mPFC) in male mice: Role of protein kinase A (PKA). *Horm. Behav.* **66**, 247–256 (2014).
32. D. Feldmeyer, B. Sakmann, Synaptic efficacy and reliability of excitatory connections between the principal neurones of the input (layer 4) and output layer (layer 5) of the neocortex. *J. Physiol.* **525**, 31–39 (2000).
33. G. Ji, V. Neugebauer, Pain-related deactivation of medial prefrontal cortical neurons involves mGluR1 and $GABA_A$ receptors. *J. Neurophysiol.* **106**, 2642–2652 (2011).
34. T. Kiritoshi, G. Ji, V. Neugebauer, Rescue of impaired mGluR5-Driven endocannabinoid signaling restores prefrontal cortical output to inhibit pain in arthritic rats. *J. Neurosci.* **36**, 837–850 (2016).
35. D. Radzicki, S. L. Pollema-Mays, A. Sanz-Clemente, M. Martina, Loss of M1 receptor dependent cholinergic excitation contributes to mPFC deactivation in neuropathic pain. *J. Neurosci.* **37**, 2292–2304 (2017).
36. J. Huang, V. M. Gadotti, L. Chen, I. A. Souza, S. Huang, D. Wang, C. Ramakrishnan, K. Deisseroth, Z. Zhang, G. W. Zamponi, A neuronal circuit for activating descending modulation of neuropathic pain. *Nat. Neurosci.* **22**, 1659–1668 (2019).
37. A. K. Jones, S. W. Derbyshire, Reduced cortical responses to noxious heat in patients with rheumatoid arthritis. *Ann. Rheum. Dis.* **56**, 601–607 (1997).
38. E. A. Mayer, S. Berman, B. Suyenobu, J. Labus, M. A. Mandelkern, B. D. Naliboff, L. Chang, Differences in brain responses to visceral pain between patients with irritable bowel syndrome and ulcerative colitis. *Pain* **115**, 398–409 (2005).
39. D. A. Seminowicz, M. Moayedi, The dorsolateral prefrontal cortex in acute and chronic pain. *J. Pain* **18**, 1027–1035 (2017).

40. G. Q. Wang, C. Cen, C. Li, S. Cao, N. Wang, Z. Zhou, X. M. Liu, Y. Xu, N. X. Tian, Y. Zhang, J. Wang, L. P. Wang, Y. Wang, Deactivation of excitatory neurons in the prelimbic cortex via Cdk5 promotes pain sensation and anxiety. *Nat. Commun.* **6**, 7660 (2015).
41. Y. Jin, Q. Meng, L. Mei, W. Zhou, X. Zhu, Y. Mao, W. Xie, X. Zhang, M.-H. Luo, W. Tao, H. Wang, J. Li, J. Li, X. Li, Z. Zhang, A somatosensory cortex input to the caudal dorsolateral striatum controls comorbid anxiety in persistent pain. *Pain* **161**, 416–428 (2020).
42. X. Zhu, H.-D. Tang, W.-Y. Dong, F. Kang, A. Liu, Y. Mao, W. Xie, X. Zhang, P. Cao, W. Zhou, H. Wang, Z. Farzinpour, W. Tao, X. Song, Y. Zhang, T. Xue, Y. Jin, J. Li, Z. Zhang, Distinct thalamocortical circuits underlie allodynia induced by tissue injury and by depression-like states. *Nat. Neurosci.* **24**, 542–553 (2021).
43. R. P. Vertes, Differential projections of the infralimbic and prelimbic cortex in the rat. *Synapse* **51**, 32–58 (2004).
44. K. Manoocheri, A. G. Carter, Rostral and caudal basolateral amygdala engage distinct circuits in the prelimbic and infralimbic prefrontal cortex. *eLife* **11**, e82688 (2022).
45. G. Capuzzo, S. B. Floresco, Prelimbic and infralimbic prefrontal regulation of active and inhibitory avoidance and reward-seeking. *J. Neurosci.* **40**, 4773–4787 (2020).
46. Y. W. Ji, Z. L. Shen, X. Zhang, K. Zhang, T. Jia, X. Xu, H. Geng, Y. Han, C. Yin, J. J. Yang, J. L. Cao, C. Zhou, C. Xiao, Plasticity in ventral pallidal cholinergic neuron-derived circuits contributes to comorbid chronic pain-like and depression-like behaviour in male mice. *Nat. Commun.* **14**, 2182 (2023).
47. T. H. Wu, L. Y. Hu, T. Lu, P. M. Chen, H. J. Chen, C. C. Shen, C. H. Wen, Risk of psychiatric disorders following trigeminal neuralgia: A nationwide population-based retrospective cohort study. *J. Headache Pain* **16**, 64 (2015).
48. J. M. Zakrzewska, J. Wu, M. Mon-Williams, N. Phillips, S. H. Pavitt, Evaluating the impact of trigeminal neuralgia. *Pain* **158**, 1166–1174 (2017).
49. A. Meulders, Fear in the context of pain: Lessons learned from 100 years of fear conditioning research. *Behav. Res. Ther.* **131**, 103635 (2020).
50. J. W. S. Vlaeyen, G. Crombez, Behavioral conceptualization and treatment of chronic pain. *Annu. Rev. Clin. Psychol.* **16**, 187–212 (2020).
51. Q. Ma, A functional subdivision within the somatosensory system and its implications for pain research. *Neuron* **110**, 749–769 (2022).
52. M. J. Henckens, J. M. Deussing, A. Chen, Region-specific roles of the corticotropin-releasing factor-urocortin system in stress. *Nat. Rev. Neurosci.* **17**, 636–651 (2016).
53. W. Tang, D. Zhou, S. Wang, S. Hao, X. Wang, M. Helmy, J. Zhu, H. Wang, CRH neurons in the laterodorsal tegmentum mediate acute stress-induced anxiety. *Neurosci. Bull.* **37**, 999–1004 (2021).
54. A. Uribe-Marino, N. C. Gassen, M. F. Wiesbeck, G. Balsevich, S. Santarelli, B. Solfrank, C. Dournes, G. R. Fries, M. Masana, C. Labermeier, X. D. Wang, K. Hafner, B. Schmid, T. Rein, A. Chen, J. M. Deussing, M. V. Schmidt, Prefrontal cortex corticotropin-releasing factor receptor 1 conveys acute stress-induced executive dysfunction. *Biol. Psychiatry* **80**, 743–753 (2016).
55. Z. Merali, P. Kent, L. Du, P. Hrdina, M. Palkovits, G. Faludi, M. O. Poulter, T. Bedard, H. Anisman, Corticotropin-releasing hormone, arginine vasopressin, gastrin-releasing peptide, and neuromedin B alterations in stress-relevant brain regions of suicides and control subjects. *Biol. Psychiatry* **59**, 594–602 (2006).
56. Q. Y. Meng, X. N. Chen, D. L. Tong, J. N. Zhou, Stress and glucocorticoids regulated corticotropin releasing factor in rat prefrontal cortex. *Mol. Cell. Endocrinol.* **342**, 54–63 (2011).
57. Z. Nie, P. Schweitzer, A. J. Roberts, S. G. Madamba, S. D. Moore, G. R. Siggins, Ethanol augments GABAergic transmission in the central amygdala via CRF1 receptors. *Science* **303**, 1512–1514 (2004).
58. T. L. Kash, D. G. Winder, Neuropeptide Y and corticotropin-releasing factor bi-directionally modulate inhibitory synaptic transmission in the bed nucleus of the stria terminalis. *Neuropharmacology* **51**, 1013–1022 (2006).
59. B. A. Strange, M. P. Witter, E. S. Lein, E. I. Moser, Functional organization of the hippocampal longitudinal axis. *Nat. Rev. Neurosci.* **15**, 655–669 (2014).
60. K. Lothmann, J. Deitersen, K. Zilles, K. Amunts, C. Herold, New boundaries and dissociation of the mouse hippocampus along the dorsal-ventral axis based on glutamatergic, GABAergic and catecholaminergic receptor densities. *Hippocampus* **31**, 56–78 (2021).
61. A. Beletskiy, E. Positselskaya, A. K. Vinarskaya, Y. S. Spivak, Y. V. Dobryakova, I. Tyulenev, V. A. Markevich, A. P. Bolshakov, Detailed analysis of dorsal-ventral gradients of gene expression in the hippocampus of adult rats. *Int. J. Mol. Sci.* **23**, 9948 (2022).
62. G. Grigoryan, M. Segal, Lasting differential effects on plasticity induced by prenatal stress in dorsal and ventral hippocampus. *Neural Plast.* **2016**, 2540462 (2016).
63. M. S. Fanselow, H. W. Dong, Are the dorsal and ventral hippocampus functionally distinct structures? *Neuron* **65**, 7–19 (2010).
64. S. Khanna, Dorsal hippocampus field CA1 pyramidal cell responses to a persistent versus an acute nociceptive stimulus and their septal modulation. *Neuroscience* **77**, 713–721 (1997).
65. H. Y. Sheng, S. S. Lv, Y. Q. Cai, W. Shi, W. Lin, T. T. Liu, N. Lv, H. Cao, L. Zhang, Y. Q. Zhang, Activation of ventrolateral orbital cortex improves mouse neuropathic pain-induced anxiodepression. *JCI Insight* **5**, e133625 (2020).

Acknowledgments: We thank Q. Ma (Westlake University) for critical reading and suggesting on the manuscript. We thank M. He (Fudan University) for giving VIP-Cre mice. **Funding:** This work was supported by Science and Technology Innovation (STI) 2030-Major Projects (2021ZD0203200-05), National Natural Science Foundation of China (82130032, 31930042, and 82021002), Shanghai Municipal Science and Technology Major Project (no. 2018SHZDZX01), and ZJLab and Shanghai Center for Brain Science and Brain-Inspired Technology. **Author contributions:** Conceptualization: Y.-Q.Z. and S.-S.L. Methodology: S.-S.L., G.-H.W., Y.-Q.C., N.L., and Y.-Q.Z. Investigation: S.-S.L., X.-J.L., Y.-Q.C., X.-Y.H., Z.-Z.Z., and L.-Q.C. Visualization: S.-S.L., X.-J.L., Y.-Q.C., and G.-H.W. Supervision: Y.-Q.Z. Writing—original draft: S.-S.L. and Y.-Q.Z. Writing—review and editing: S.-S.L. and Y.-Q.Z. **Competing interests:** The authors declare that they have no competing interests. **Data and materials availability:** All data needed to evaluate the conclusions in the paper are present in the paper and/or the Supplementary Materials.

Submitted 27 June 2023
Accepted 21 December 2023
Published 19 January 2024
10.1126/sciadv.adj4196